Intrinsic optical intersubband bistability in quantum well structures: Role of multiple reflections

Victor Bondarenko[1,*] and Mirosław Załużny[2]

[1]*Institute of Physics, National Academy of Sciences of Ukraine, prospect Nauky 46, Kyiv 03028, Ukraine*

[2]*Institute of Physics, Maria Curie-Skłodowska University, Pl. M. Curie-Skłodowskiej 1, 20-031 Lublin, Poland*

(Received 9 June 2014; revised manuscript received 7 December 2014; published 8 January 2015)

We theoretically investigate the nonlinear intersubband response, in particular the intrinsic optical bistability (IOB), of quantum well (QW) structures embedded into layered systems. A semiclassical approach is employed based on the plane-wave approximation, the transfer-matrix formalism, the sheet model, and the density-matrix formalism developed to calculate the two-dimensional nonlinear intersubband electron conductivity and the IOB. A variety of presented numerical results demonstrate the importance of inhomogeneity of spatial distribution of radiation intensity induced by multiple radiation reflection for the IOB in layered structures. It is shown that knowing the radiation intensity distribution in the area occupied by QWs, in part standing-wave patterns, are crucial for understanding of IOB pictures. The IOB in systems of one, two, three, five, and ten QWs is investigated. The multistability phenomenon is addressed.

DOI: 10.1103/PhysRevB.91.035303 PACS number(s): 42.65.Pc, 42.70.Nq, 73.21.Fg, 78.30.Fs

I. INTRODUCTION

Intrinsic optical bistability (IOB) due to intersubband transitions in quantum well (QW) structures has attracted a genuine interest due to its intriguing nature and a possibility of practical applications. Optical bistability (OB) requires positive feedback in the system. Contrary to the mirror-based optical bistability (MOB) when the feedback is provided externally by means of microcavity (MC) mirrors (see, e.g., Refs. [1,2]), the IOB phenomenon is based on the fact that the positive feedback in the system is provided not externally but by a strongly nonlinear element that is intrinsic to the system. In the considered in this paper QW systems, it is the direct dynamic electron-electron (*e-e*) interaction [3] that provides the feedback. The term "dynamic *e-e* interaction" labels interaction between electrons involved in the intersubband transitions contrary to the interaction between stationary nontransiting electrons that is labeled by the term "static *e-e* interaction." Substantial influence of the dynamic *e-e* interaction on the nonlinear intersubband response has been observed by Craig *at al.* [4] (in single QW) employing wave guide configuration.

Practically, in all papers discussing the intrinsic optical intersubband bistability (see, e.g., Refs. [3,5–10]) the authors considered systems containing a single QW assuming additionally that intensity of the field in the QW coincided with intensity of the incident field. Such a simplification is equivalent to neglecting the light reflection from different interfaces as well as from the quasi-two-dimensional electron gas (Q2DEG) located in the QW [11,12]. The role of the reflections was partially discussed in Refs. [13,14] where the cavity-induced enhancement of the intrinsic intersubband bistability was studied. However, in Ref. [14] the authors considered (employing an iteration method) rather exotic systems when growth direction of multiple QWs (MQWs) located inside MC was parallel to the mirrors. On the other hand, in Ref. [13], where influence of MC on the IOB for a single QW inside a semiconductor MC was studied, the author took into account only the third-order nonlinearity and additionally neglected the difference between dephasing and depopulation rates. That makes reliability of the reported results quite questionable.

In this paper, we consider the IOB response of a single QW and MQW (embedded into multilayer systems) beyond the above-mentioned approximations. We concentrate on two typical configurations, namely, (i) the total internal reflection (TIR) configuration (see, e.g., Refs. [15,16] where intersubband absorption saturation in MQW was experimentally studied) and (ii) the configuration in which MQW is embedded into a semiconductor MC (MQW-MC system). The TIR configuration is realized for MQW in half-MC (MQW-HMC systems). In such layered systems, the effect of multiple light reflections from different interfaces and the Q2DEG is more significant on the nonlinear response than on the linear response [11,12,15–17]. Thus, a bistability response of QWs in layered systems is expected to be much richer (including a multistability) than the one of a QW system without multiple reflections (i.e., embedded in an infinite uniform environment). We should also remember that in the case of MQW-MC systems under a strong coupling regime formation of the polariton branches affects substantially the nonlinear response (see, e.g., Ref. [18] where the *e-e* was omitted). Detailed discussion of the polariton issue in the presence of the *e-e* interaction is beyond the scope of this paper.

One of the key parameters driving the IOB in MQW embedded into a layered system is the radiation intensity in the region occupied by each QW. To provide the IOB in an individual QW, the radiation intensity in its area is supposed to belong to a certain interval. The complexity of the IOB problem for MQW stems from the fact that due to light reflection, in part from the Q2DEG, the radiation intensity in a given QW depends on the radiation intensity in all other QWs, thus making the QWs electromagnetically coupled [12]. The multiple light reflection at different interfaces introduces substantial inhomogeneity of the spatial distribution of the light intensity in the area occupied by QWs. For example, in the case of typical TIR geometry, we observe formation of the

*ai8868@wayne.edu

standing-wave pattern that essentially affects the (saturated) nonlinear response [15]. The spatial modulation of the light field allows for manipulation of light-matter interaction. By locating QWs with respect to the antinodes and nodes of the light field, we can modify the radiative coupling of the QWs. In this context, the following questions arise: How does the interwell distance interplay with location of QWs in the standing-wave pattern? Can IOB pictures in the considered systems be predictable? This becomes an issue of vital importance for applications.

The complexity of interdependence requires the calculation procedure for the radiation intensity in MQWs to be self-consistent. The level of difficulty can be understood if we assume, for example, that the IOB occurs in one QW of a two-QW system. It means that there are three real values for some physical quantity in that QW and the radiation intensity in the other radiative coupled QW depends not on one, but on all the three values of that physical quantity. If each of two radiative coupled QWs has three real values for some physical quantity, then it means that the three values in one QW depend on the three values in the other QW and vice versa. What if the number of radiative coupled QWs is large ($\gtrsim$10)? One can reasonably expect this issue to be a major challenge for computer codes.

To solve those problems, we apply the transfer-matrix approach for the light propagation in the considered layered systems. The sheet model developed to calculate two-dimensional (2D) nonlinear intersubband electron conductivity and the IOB in the Q2DEG is employed. In general, the IOB of the Q2DEG is described by equations that allow three different real roots for some physical quantity assigned to the system for a certain set of parameters of that system. The equations could be transcendental or cubic. Cubic equations (see, e.g., Refs. [5,8,19]) are easier to deal with and they may allow more extensive analytical investigation than transcendental ones. That makes models with a cubic equation, if they are possible at all, more preferable. Even cubic equations differ in their complexity. We apply an approach to obtain a simpler and easier to use cubic equation. Under the IOB regime, the parameters of the system become strongly interdependent, that is, tied to each other by those equations and their solutions. It means that there are some narrow intervals of values for those parameters which depend on each other when the IOB can take place. As shown in Ref. [19] (see also Ref. [8]), the IOB in a two-subband system under certain circumstances can be described by a rather simple cubic equation with a set of five interdependent dimensionless parameters: normalized radiation intensity in the system, normalized matrix element of the potential of the electron-electron interaction, detuning parameter, and normalized dephasing and relaxation times. By modifying the recursion approach developed in our previous paper [20], we have built a computer code that solves the problem when under intensive incident radiation there are three different real values for the distribution of electrons between the ground and the first excited subbands in each QW of MQW systems. Thus, on the one hand, the code takes into account multiple reflections and light absorption by Q2DEG, and on the other hand, it allows for obtaining as stable as nonstable solutions of the IOB process. (We would like to stress that we consider only electromagnetically coupled QWs in MQW structures with rather wide barriers that prevent coupling of electron states of QWs.)

In the following Sec. II we present theoretical background describing our model and, in particular, our approach to treatment of the IOB in Sec. II B. Section III is devoted to discussion of the results of our numerical calculations performed for the MQW-HMC (Sec. III A) and MQW-MC (Sec. III B) geometries. Interpretation of various IOB pictures, in particular the IOB pictures with 8-like and O-like curves, is concentrated in Sec. III C. Section III D is to shed light on basic details of how the IOB pictures are produced by the Q2DEG and modified by multiple radiation reflection. Section IV contains conclusions.

II. THEORETICAL BACKGROUND

A. Transfer-matrix approach and sheet model

Our system of interest is a layered structure located between substrate ($j = 0$) and cladding ($j = m + 1$) media with the dielectric constant $\varepsilon_0 = \varepsilon_s$ and $\varepsilon_{m+1} = \varepsilon_c$, respectively, where j counts the layers of the structure. The substrate and cladding are nonabsorptive semi-infinite media. The incident radiation field is assumed to be represented by a monochromatic plane wave of frequency ω. The radiation incidents from the substrate medium at the angle φ with respect to the optic axis z parallel to the growth direction of the structure (see Fig. 1).

We assume that the radiation is polarized in the $x - z$ plane. Then, there is the only nonzero component of the magnetic field $\mathbf{H}(\mathbf{r},t) = \mathbf{e}_y H_y(z) e^{\mathrm{i}(k_x x - \omega t)}$ in each medium where $k_x = \sin(\varphi)\omega\sqrt{\varepsilon_s}/c$ is the in-plane wave vector. The complex amplitudes of the magnetic field corresponding to the waves traveling in the positive (+) and negative (−) z directions are denoted by $H^{(j)}_{\alpha+}$ and $H^{(j)}_{\alpha-}$, respectively, with $\alpha = l,u$. The subscript l (u) indicates that the amplitude is taken with respect to the plane separating the media j and $j + 1$ ($j - 1$ and j).

The Q2DEG in a QW is modeled by a 2D sheet. (For convenience, we neglect intrasubband excitation and assume that QWs are symmetric and rectangular.) The sheets are positioned at the centers of the QWs (at $z = z_{\mathcal{N}}$, $\mathcal{N} = 1,2,3 \ldots N_{\mathrm{QW}}$ and N_{QW} is the number of QWs). The Q2DEG in the $\mathcal{N}$th QW is characterized by the 2D intersubband conductivity $\sigma^{2\mathrm{D}}_{zz}$ that depends on ω and the normal component

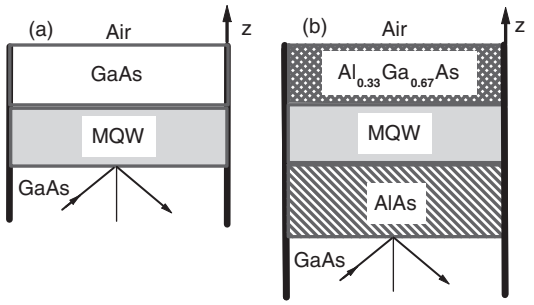

FIG. 1. Schematics for the geometries of the two systems discussed in the paper: (a) the MQW-HMC structure and (b) the MQW-MC structure.

of the electric field amplitude $|E_z^{(\mathcal{N})}| = |E_z(z = z_{\mathcal{N}})|$ in that QW [20].

Relation between amplitudes of the magnetic field in the q and $p(> q+1)$ media which are layers may be written in terms of the transfer matrix [17]

$$\begin{bmatrix} H_{l+}^{(q)} \\ H_{l-}^{(q)} \end{bmatrix} = \mathbf{I}_{q,q+1} \prod_{j=q+1}^{p-1} \mathbf{L}_j \mathbf{I}_{j,j+1} \begin{bmatrix} H_{u+}^{(p)} \\ H_{u-}^{(p)} \end{bmatrix}. \quad (1)$$

The matrix $\mathbf{L}_j$ describes the propagation effect through the jth layer, while the matrix $\mathbf{I}_{i,j}$ accounts for the interface between neighboring homogeneous media (layers) i and $j(= i+1)$. The transfer matrix $\mathbf{I}_{i,j}(\equiv \mathbf{I}_{\mathcal{N}})$ across the $\mathcal{N}$th sheet can be written in terms of the amplitude reflection coefficient $r_{\mathcal{N}}^{2D}$ and amplitude transmission coefficient $t_{\mathcal{N}}^{2D}$ of the $\mathcal{N}$th sheet which are connected with the conductivity σ_{zz}^{2D} by the relations [17,20]

$$r_{\mathcal{N}}^{2D} = (\Lambda_{\mathcal{N}}/2)/[1 + (\Lambda_{\mathcal{N}}/2)], \quad (2)$$

$$t_{\mathcal{N}}^{2D} = 1 - r_{\mathcal{N}}^{2D} = 1/[1 + (\Lambda_{\mathcal{N}}/2)], \quad (3)$$

where

$$\Lambda_{\mathcal{N}} \equiv \Lambda_{QW}(\omega, \varphi_w, I^{(\mathcal{N})}) = (4\pi/c\sqrt{\varepsilon_w})\sigma_{zz}^{2D}\left(\omega, \left|E_z^{(\mathcal{N})}\right|\right) F(\varphi_w), \quad (4)$$

with $F(\varphi_w) = \tan\varphi_w \sin\varphi_w$, $\varphi_w = \arcsin[(\varepsilon_w/\varepsilon_s)^{1/2} \sin\varphi]$, and ε_w is the dielectric constant of the QW material.

The intensity-dependent reflectance amplitude of the multilayer structure is defined as

$$r = H_{l-}^{(0)}/H_{l+}^{(0)}. \quad (5)$$

It can be calculated analytically only in particular cases making appropriate simplifications. In general, calculation of the reflectance requires a numerical approach. We employ the recursion method that was developed in our previous paper [20] for the system where the dynamic e-e interaction played a negligible role. In this work, the method is modified in such a way that when solving our Eq. (9) for each individual QW (at every recursion step), we take into account all possible solutions (stable as well as unstable) of (9) (see following).

B. 2D nonlinear intersubband conductivity and intrinsic optical bistability

2D nonlinear intersubband electron conductivity for an individual QW at the location z that appears in Eq. (4) is calculated within the density-matrix formalism under the stationary condition. Restricting to the two-subband limit and the rotating-wave approximation (RWA), we find that

$$\sigma_{zz}^{2D}(\omega, \tilde{I}_z) = \frac{-ie^2 f_{2\to1} N_S}{2m^*} \frac{\triangle\rho_{12}(\omega, \tilde{I}_z)}{\bar{E}_{21}(\omega, \tilde{I}_z) - \hbar\omega - i\gamma_{IT}}. \quad (6)$$

Here, N_S is the 2D electron density, $f_{1\to2} = 2m^* E_{21}|z_{12}|^2/\hbar^2$ is the oscillator strength associated with electron transitions between the first (the ground) and the second (the first excited) subbands ($1 \to 2$ transitions), $E_{21} = E_2 - E_1$ is the energy gap between the second and the first subbands, $-ez_{12}$ is the intersubband dipole matrix element, with $-e$ and m^* being the charge and effective mass of the electron, $\hbar$ the Plank constant, and $i = \sqrt{-1}$. Radiation intensity at the location z enters Eq. (6) by means of the dimensionless parameter $\tilde{I}_z = |E_z/E_z^{sat}|^2$ where $E_z^{sat} = \hbar(\gamma_{IT}\Gamma_{IT})^{1/2}/|ez_{12}|$. γ_{IT} is the phenomenological dephasing rate and Γ_{IT} is the phenomenological decay rate of the excited state in the QW. Note that, contrary to γ_{IT}, Γ_{IT} enters the expression for σ_{zz}^{2D} only through $\tilde{I}_z$.

In Eq. (6), $\triangle\rho_{12}(\omega, \tilde{I}_z) = \rho_{11}(\omega, \tilde{I}_z) - \rho_{22}(\omega, \tilde{I}_z)$ where $\rho_{11}(\omega, \tilde{I}_z)$ and $\rho_{22}(\omega, \tilde{I}_z)$ stand for the diagonal elements of the density matrix. The radiation intensity-dependent 2D electron population of the jth subband is given by $N_S\rho_{jj}(\omega, \tilde{I}_z)$. The difference between the 2D electron populations of the first and the second subbands is $N_S\triangle\rho_{12}(\omega, \tilde{I}_z)$, which represents the degree of excitation of the QW due to the intensive radiation.

In Eq. (6), $\bar{E}_{21}$ is the intersubband resonant energy of the considered QW. It is larger than the bare intersubband energy E_{21} due to the dynamic e-e interaction and dependence on the degree of excitation of the QW caused by the incident radiation. In the approximation used here, it takes the form

$$\bar{E}_{21}(\omega, \tilde{I}_z) = E_{21}[1 + \triangle\rho_{12}(\omega, \tilde{I}_z)V_{21}/E_{21}], \quad (7)$$

where the dynamic e-e interaction due to the $1 \to 2$ electron transitions is represented by the parameter

$$V_{21} = \frac{e^2 N_S L_{1,2;1,2}}{\varepsilon_w \varepsilon_0}. \quad (8)$$

The Coulomb matrix element $L_{1,2;1,2} = \int_{-\infty}^{\infty} dz[\int_{-\infty}^{z} dz' \chi_1(z')\chi_2(z')]^2$, with $\chi_j(z)$ the z-dependent electron wave function for the jth subband.

The quantity $\triangle\rho_{12}(\omega, \tilde{I}_z)V_{21}/E_{21}$ in Eq. (7) defines the intensity-dependent depolarization shift (normalized by E_{21}) in the QW. It is important to note that in this paper the dependence of $\chi_{1(2)}$ and E_{21} on the redistribution of electrons between the subbands is neglected. It has a good justification in the case of the rectangular QWs [3,8].

In further discussion we assume for simplicity that in the absence of the radiation only the ground subband is occupied, i.e., $\triangle\rho_{12}(\omega, \tilde{I}_z = 0) \equiv \triangle\rho_{12}^{(0)} = 1$. Using the approach of Refs. [19] and [8] we obtain that $\triangle\rho_{12}(\omega, \tilde{I}_z)$ is governed by the following nondimensional cubic equation:

$$(\triangle\rho_{12})^3 + a(\triangle\rho_{12})^2 + b(\triangle\rho_{12}) + c = 0, \quad (9)$$

where

$$a = 2(\tilde{\delta}_{21}/\tilde{V}_{21}) - 1, \quad (10)$$

$$b = \left(\frac{\tilde{\gamma}_{IT}}{\tilde{V}_{21}}\right)^2 (1 + \tilde{I}_z) - 2\frac{\tilde{\delta}_{21}}{\tilde{V}_{21}} + \left(\frac{\tilde{\delta}_{21}}{\tilde{V}_{21}}\right)^2, \quad (11)$$

and

$$c = -\left[\left(\frac{\tilde{\gamma}_{IT}}{\tilde{V}_{21}}\right)^2 + \left(\frac{\tilde{\delta}_{21}}{\tilde{V}_{21}}\right)^2\right]. \quad (12)$$

For convenience, we have introduced the following nondimensional parameters:

$$\tilde{\delta}_{21} = (E_{21} - \hbar\omega)/E_{21}, \quad (13)$$

$$\tilde{V}_{21} = V_{21}/E_{21}, \quad (14)$$

$$\tilde{\gamma}_{IT} = \gamma_{IT}/E_{21}. \quad (15)$$

The factors a, b, and c here have simpler forms than in Ref. [19] due to neglecting the nonresonant elements of the density matrix within the RWA. Note that Eqs. (9)–(12) coincide with the cubic equation and its factors [Eqs. (6) and (7)] in Ref. [8].

Equation (9) always has one real root and it can have three different real roots under certain strict general conditions [8]. When (9) has three different real roots it determines conditions for the IOB in the two-subband system. We would like to emphasize that Eq. (9) is cubic only because $\tilde{V}_{21} \neq 0$ which means that the IOB cannot take place if there is no dynamic e-e interaction incorporated in the picture.

When the interaction is neglected, i.e., $\tilde{V}_{21} = 0$, Eq. (9) reduces to

$$\triangle\rho_{12} = \frac{\triangle\rho_{12}^{(0)}}{1+\tilde{I}_z}, \tag{16}$$

which becomes exactly Eq. (16) in Ref. [21] if $\gamma_{\rm IT} = \Gamma_{\rm IT}$ is assumed. The above expression represents in the simplest form the saturation phenomenon. Equation (9) shows that the saturation phenomenon is affected by the dynamic e-e interaction and the effect can be considerable.

It is instructive to investigate a particular case when $\tilde{\delta}_{21} = 0$. Then, the cubic equation (9) takes a reduced form

$$(\triangle\rho_{12})^2\,(1-\triangle\rho_{12})\,\mathcal{P}_{12} = \triangle\rho_{12}(1+\tilde{I}_z) - \triangle\rho_{12}^{(0)}. \tag{17}$$

Equation (17) clearly shows that the quantity $\mathcal{P}_{12} = (\tilde{V}_{21}/\tilde{\gamma}_{\rm IT})^2$ controls the effect of the dynamic e-e interaction on the saturation process as we have stated above. [When $\mathcal{P}_{12} \ll 1$ ($\mathcal{P}_{12} \gtrsim 1$), then the e-e interaction effect is negligibly small (substantial).] The nonzero value of V_{21} makes Eq. (17) cubic. Therefore, $\mathcal{P}_{12}$ can serve as a parameter whose certain values can let Eq. (17) have three different real roots that represent the IOB.

It is very handy to have one parameter instead of three combined parameters a, b, and c [see Eqs. (9)–(12)] while searching the numerical conditions for the IOB. The immediate result of this analysis is that to provide the IOB the value of $\mathcal{P}_{12}$ is supposed to be taken larger than one. That condition may be a challenge for realistic systems, particularly in the case of thin QWs with $E_{21} \gtrsim 100$ meV. It is reasonable to expect that the values of $\tilde{\delta}_{21}$ that can be appropriate for the cubic equation (9) to have three different real roots could be sought around zero, including negative, positive, and zero values.

It should be emphasized that providing a cubic equation for $\triangle\rho_{12}$ like Eq. (9) and having three different real roots of that equation are necessary conditions for observing the IOB. Nevertheless, we should remember that the ultimate IOB picture is controlled by the intensity-dependent 2D conductivity or more precisely by the quantity $\Lambda_{\rm QW}$ in expressions for the reflection and transmission amplitudes of the Q2DEG [see Eqs. (2), (3), and (4)]. Employing Eqs. (4) and (6), one finds that $\Lambda_{\rm QW}$ can be written as

$$\Lambda_{\rm QW} = \frac{\Lambda_0 F(\varphi)\triangle\rho_{12}}{(\triangle\rho_{12}\tilde{V}_{21}+\tilde{\delta}_{21})/\tilde{\gamma}_{\rm IT} - i}, \tag{18}$$

where $\Lambda_0 = 2\pi e^2 f_{2\to1}\hbar N_S/(m^* c\sqrt{\varepsilon_w}\gamma_{\rm IT})$. Taking typical for GaAs values of $m^* = 0.066\,m_0$ and $\varepsilon_w = 10.89$, we find that $\Lambda_{0|\rm GaAs} = 0.16\times f_{2\to1} N_s[10^{12}\ {\rm cm}^{-2}]/\gamma_{\rm IT}[{\rm meV}]$.

Equation (18) manifests a vital resonant role of the $\tilde{I}_z$-dependent depolarization shift (more precisely the bistable behavior of $\triangle\rho_{12}$) for the IOB process [19]. Numerical simulations (see, e.g., Fig. 1 in Ref. [8]) indicate that slightly negative values for $\tilde{\delta}_{21}$ may be more preferable to provide (more pronounced) IOB pictures. In other words, $\hbar\omega$ is supposed to be slightly larger than E_{21} to observe sound IOB phenomena.

Equations (2) and (18) give the following expression for reflectance of one sheet of Q2DEG with small $\Lambda_{\rm QW}$ embedded into an infinite dielectric medium with dielectric constant ε_w (the transmission geometry):

$$R^{\rm inf}_{N_{\rm QW}=1} = \left(\frac{\Lambda_0 F(\varphi)}{2}\right)^2 \frac{\triangle\rho_{12}^2}{[(\triangle\rho_{12}\tilde{V}_{21}+\tilde{\delta}_{21})/\tilde{\gamma}_{\rm IT}]^2+1}. \tag{19}$$

Assuming that influence of the light reflection and light absorption by Q2DEG on the light redistribution in the layered systems is rather small, it is instructive to approximate reflectance of MQW-HMC for the TIR geometry and MQW-MC by the analogous to the linear case [17] expression

$$R^{\rm appr}_{\rm MQW} = 1 - \sum_{\mathcal{N}=1}^{N_{\rm QW}} {\rm Re}\Lambda_{\rm QW}\big(\omega,\varphi_w,\tilde{I}_z^{(\mathcal{N})}\big)\mathcal{R}_z^{(\mathcal{N})}, \tag{20}$$

where $\mathcal{R}_z^{(\mathcal{N})} = \tilde{I}_z^{(\mathcal{N})}/\tilde{I}_{\rm inc}\sin^2\varphi_w$. The term ${\rm Re}\Lambda_{\rm QW}(\omega,\varphi_w,\tilde{I}_z^{(\mathcal{N})})$ produces an S-like curve of the IOB derived from the conductivity in the $\mathcal{N}$th QW. Ratio $\mathcal{R}_z^{(\mathcal{N})}$ represents the effect of the light reflection in the layered structure, in particular from the mirror of MC. For MQW-HMC, the ratio can be evaluated by the standing-wave pattern. $\mathcal{R}_z^{(\mathcal{N})}$ for MQW-MC stands for a more complicated cavity enhancement factor. In part, the ratio is responsible for an S-like curve for reflectance under the MOB regime when QWs in a microcavity do not feature the IOB. Equation (20) is able to illustrate a combined effect of the IOB and MOB in MQW-MC as well. Cooperation or battle of S-like curves for the IOB and an S-like curve for the MOB can yield quite a confusing outcome. Equations (19) and (20) show that during the IOB, reflection of one-QW system rises for the transmission geometry and falls for the TIR geometry and MC.

It is important to stress that deriving Eq. (9) we have assumed the dephasing rate $\gamma_{\rm IT}$ to be unaffected by the light-induced repopulation of the subbands. However, when $\triangle\rho_{12}(\omega,\tilde{I}_z)$ differs considerably from 1 it changes $\gamma_{\rm IT}$ (at large electron concentration) [22,23]. Influence of this additional nonlinear phenomenon on the IOB has not been investigated yet. It will be discussed elsewhere. Here, we only note that in general this phenomenon makes Eq. (9) a transcendental equation that dramatically complicates analysis.

III. NUMERICAL RESULTS AND DISCUSSION

In this section, we present numerical results and their discussion for the systems schematically shown in Fig. 1. To avoid confusion in the following we distinguish the dimensionless parameter $\tilde{I}_z(z=z_{\mathcal{N}}) = \tilde{I}_z^{(\mathcal{N})}$ in the expression for the nonlinear conductivity (6) for an individual QW at the location $z = z_{\mathcal{N}}$ from the normalized intensity defined as $\tilde{I}_{\rm inc} = |E_{\rm inc}/E_z^{\rm sat}|^2$ where $E_{\rm inc}$ is the electric field amplitude

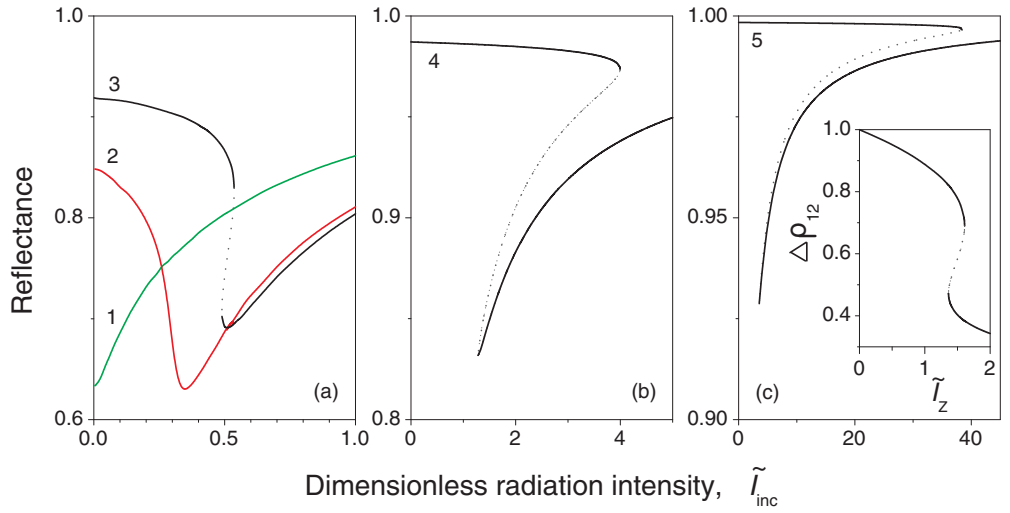

FIG. 2. (Color online) Dependence of reflectance on the dimensionless incident radiation intensity $\tilde{I}_{\rm inc}$ for GaAs-QW-GaAs(1.9 μm)-air structure with constant $N_S = 8\times10^{11}$ cm^{-2} for different $\mathcal{V}_{21}$ [$\tilde{V}_{21}$]: (1) 0.0125 [0.01], (2) 0.05 [0.04], (3) 0.0625 [0.05], (4) 0.125 [0.1], and (5) 0.3125 [0.25]. $d_{\rm QW} = 90$ Å and $d_{\rm B} = 300$ Å. In the inset: solution $\triangle\rho_{12}$ of the cubic equation (9) as a function of the dimensionless radiation intensity $\tilde{I}_z$ in a QW with $\tilde{V}_{21} = 0.05$. Solid and dotted lines represent stable and unstable solutions, respectively.

of the radiation that incidents on the substrate of the entire structure. $\tilde{I}_{\rm inc}$ is an input numerical parameter in our calculations. $\tilde{I}_z$ in each QW depends on $\tilde{I}_{\rm inc}$ as well as on the light propagation, reflection, and absorption in the whole structure.

We are interested in the situation of three different real roots $\triangle\rho_{12}(\omega,\tilde{I}_z)$ of Eq. (9) that provides the IOB. In addition to the five mentioned in the introduction parameters that define the IOB in a two-subband QW, there are a few more parameters that affect $\tilde{I}_z$ and, thus, determine the IOB in MQWs in layered structures. They are the thickness of the barrier between neighbor QWs, the QW width, the thickness of the spacer layer, as well as the thickness of the low-index layer playing the role of coupling mirror. For better understanding of the microcavity and radiative coupling effects in MQW-MC systems [Fig. 1(b)], we first consider the case when MQW is located in the half microcavity where the coupling mirror is removed [Fig. 1(a)].

We assume the following parameters to be the same for all our numerical calculations. In the considered $Al_{0.33}Ga_{0.67}As$-GaAs-$Al_{0.33}Ga_{0.67}As$ quantum well structure, the thickness $d_{\rm QW}$ of the GaAs quantum well is 90 Å. Thickness of each of the $Al_{0.33}Ga_{0.67}As$ barriers for an individual QW structure is assumed to be $d_{\rm B}/2$ so that two neighbor QWs in a MQW system are separated by the barrier of $d_{\rm B}$ width and two neighbor sheets of the Q2DEG are separated by the $d_{\rm QW} + d_{\rm B}$ distance. The energy gap $E_{21} = 115$ meV. The oscillator strength $f_{1\to2} = 1$ except one case when oscillator strength $f_{1\to2} = 2$ is taken for comparison. The dephasing rate is $\gamma_{1T} = 1.1$ meV, dielectric constants of the well and the barrier are $\varepsilon_w = 10.89$ and $\varepsilon_b = 9.989$, respectively. We choose the photon energy $\hbar\omega = 117.2$ meV ($\tilde{\delta} = -0.0191$) and the angle of incidence $\varphi = 65^\circ$. We assume $\hbar\omega$ and φ to be fixed to reduce the number of parameters determining IOB pictures. The problem of how change of $\hbar\omega$ and φ affects IOB pictures will be discussed in future papers.

Thickness of the barrier $d_{\rm B}$, sheet density of electrons N_S, dimensionless parameter of the *e-e* interaction $\tilde{V}_{21}$, thickness of the spacer layer $d_{\rm SPAC}$, and the thickness of low-index layer $d_{\rm MIRR}$ are specified for each particular consideration.

We would like to make some general comments. A graph for dependence of the solution $\triangle\rho_{12}$ of the cubic equation (9) upon a single parameter $\tilde{I}_z$ in an $\tilde{I}_z$ interval where the equation has as one as three different real roots is represented by the (reverse) S-like curve in the inset in Fig. 2(c). The S-like dependence of $\triangle\rho_{12}(\tilde{I}_z)$ makes the real and imaginary parts of $\sigma_{zz}^{\rm 2D}(\tilde{I}_z)$ in Eq. (6) also S like. Being derived from the real part of the conductivity, reflectance of the system is also expected to feature S-like dependence on the radiation intensity under the IOB regime. In reality, the middle part of the S-like curve represents an unstable state and is not measurable. During the IOB process $\triangle\rho_{12}(\tilde{I}_z)$, Re$\sigma_{zz}^{\rm 2D}(\tilde{I}_z)$ and reflectance change or switch their values discontinuously (between the upper and lower parts of the S-like curves which represent stable or measurable states). We show stable and unstable states differently, by solid and dotted lines, respectively, only in Fig. 2. Also, we show possible discontinuous transitions for complicated IOB processes only in the insets in Figs. 5(b) and 12 where stable and unstable states are represented by solid and dotted lines, respectively. Merely for the sake of illustration simplicity we neither distinguish those lines nor show discontinuous transitions in the rest of the presented figures where all lines are uniform solid. We assume it is understood. Besides, sometimes it is quite a question as to what is not a measurable part of the curve representing a complicated OB process. It is also convenient for our discussion to define the short-term "depth of switch" to characterize IOB pictures, with the depth standing for the size of the discontinuous gap between switched values during the IOB; it is the distance between the upper and lower parts of the "S." The bigger depth is the more distinguished the IOB is.

The S-like curve in the inset in Fig. 2(c) represents each QW with $\tilde{V}_{21} = 0.05$ because all such QWs are assumed to

be the same. It requires the same interval, from $\tilde{I}_z^{\min} \approx 1.36$ to $\tilde{I}_z^{\max} \approx 1.6$ for $\tilde{I}_z$ (and not necessarily the same interval for $\tilde{I}_{\rm inc}$!) for every QW with the given set of parameters to feature the IOB.

The inset in Fig. 2(c) shows that when $\tilde{I}_z$ grows up from $\tilde{I}_z^{\max}$, the value of $\triangle\rho_{12}$ continuously decreases. What is the expected behavior of $\mathrm{Re}\sigma_{zz}^{\rm 2D}$ and reflectance then? In Ref. [19], it is shown that the discontinuous transitions during the IOB process realize the resonant transitions when $\triangle\rho_{12}\tilde{V}_{21} \to \tilde{\delta}_{21}$ [see also our Eq. (18)]. Therefore, beyond the area of resonant discontinuous transitions, the value of $\mathrm{Re}\sigma_{zz}^{\rm 2D}$ experiences dramatic reduction. Likewise, the reflectance is expected to demonstrate relaxation of its value from the resonant one if the radiation intensity grows farther beyond the switch area: the reflectance of one QW system rises for the TIR geometry (Secs. III A and III B) and falls for the transition geometry (Sec. III D).

When the QW is located next to the perfect metal mirror, then $\tilde{I}_z = 4\tilde{I}_{\rm inc}\sin^2\varphi$ where factor 4 appears due to the standing-wave effect. This case helps us estimate the smallest value, the threshold, for $\tilde{I}_{\rm inc}$, around 0.5, to provide an IOB picture when a QW is located at an antinode of the standing-wave pattern of the MQW-HMC systems in Sec. III A. On the other hand, $\tilde{I}_z = \tilde{I}_{\rm inc}\sin^2\varphi$ for a free-standing QW when light reflection is neglected that gives an estimated value of 1.8 for the $\tilde{I}_{\rm inc}$ threshold to provide the IOB in one QW in Sec. III D.

Along with the depth of switch and $\tilde{I}_{\rm inc}$ threshold the width of switch can be important for application. The width of switch is defined as the $\tilde{I}_{\rm inc}$ interval for the IOB to occur. We make no accent on the width of switch in our discussion and leave the matter to the reader.

A. MQW-HMC system

The numerical calculations reported in the following are performed for the following MQW-HMC system: GaAs-MQWs-GaAs-air [Fig. 1(a)] with different values for the thickness $d_{\rm SPAC}$ of the GaAs spacer layer and $d_{\rm B}$. We evaluate the effect of N_S and $\tilde{V}_{21}$ on IOB pictures. Since N_S enters expressions (6) for 2D conductivity directly and through $\tilde{V}_{21}$ [Eq. (8)], it is instructive for analysis to rewrite the dimensionless $\tilde{V}_{21}$ in the form $\tilde{V}_{21} = \mathcal{V}_{21}N_S[10^{12}\ \mathrm{cm}^{-2}]$ where $\mathcal{V}_{21}$ is a dimensionless quantity determined mainly by the material design of QWs.

1. One-QW-HMC system

Figure 2 presents the $\tilde{I}_{\rm inc}$ dependence of the reflectance of the QW-HMC structure with $d_{\rm SPAC} = 1.9\ \mu$m for different $\mathcal{V}_{21}$, and consequently $\tilde{V}_{21}$, at constant $N_S = 8\times10^{11}\ \mathrm{cm}^{-2}$. Figure 3 demonstrates the effect of different N_S at constant $\tilde{V}_{21} = 0.05$, while in the inset $\mathcal{V}_{21} = 0.125$ is assumed to be constant instead of $\tilde{V}_{21}$, for the same QW-HMC structure as in Fig. 2. Inspection of Figs. 2 and 3 shows that there are intervals for $\tilde{V}_{21}$ and $\mathcal{V}_{21}$ that provide the IOB. In part, the intervals from about 0.0625 to about 0.125 for $\mathcal{V}_{21}$ and, correspondingly, from about 0.05 to about 0.1 for $\tilde{V}_{21}$ are the most suitable to produce the most outstanding IOB pictures in the considered structure. Once $\tilde{V}_{21}$ is one of the constituents defining the $\tilde{I}_z$-dependent depolarization shift in Eq. (7), the two figures

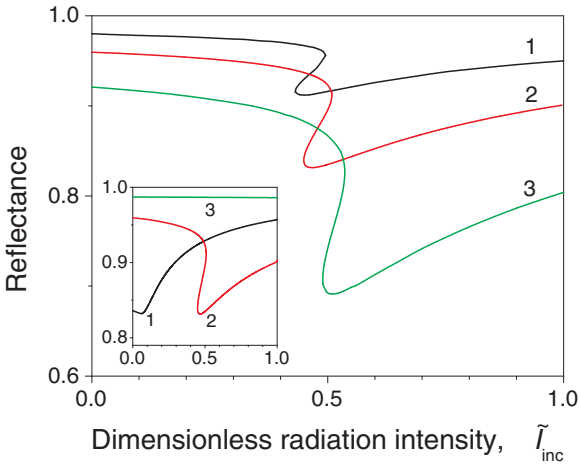

FIG. 3. (Color online) Dependence of reflectance on the dimensionless incident radiation intensity $\tilde{I}_{\rm inc}$ for GaAs-QW-GaAs(1.9 μm)-air structure with constant $\tilde{V}_{21} = 0.05$ for different N_S: (1) $N_S = 2\times10^{11}\ \mathrm{cm}^{-2}$ [$\mathcal{V}_{21} = 0.25$], (2) $N_S = 4\times10^{11}\ \mathrm{cm}^{-2}$ [$\mathcal{V}_{21} = 0.125$] and (3) $N_S = 8\times10^{11}\ \mathrm{cm}^{-2}$ [$\mathcal{V}_{21} = 0.0625$]. In the inset, $\mathcal{V}_{21} = 0.125$ is assumed to be constant instead of $\tilde{V}_{21}$. Line 3 in the inset is line 4 in Fig. 2. $d_{\rm B} = 300$ Å.

illustrate a critical role of the $\tilde{I}_z$-dependent depolarization shift for providing the IOB regime as is mentioned after Eq. (18).

In the following calculations, we assume $N_S = 8\times10^{11}\ \mathrm{cm}^{-2}$ and $\tilde{V}_{21} = 0.05$. Bearing in mind Figs. 2 and 3 (see also Fig. 1 in Ref. [8]), one can conclude that there exists a certain interval of values for N_S when the IOB exists and is the most pronounced. It is not quite excluded that the assumed value $N_S = 8\times10^{11}\ \mathrm{cm}^{-2}$ cannot support the IOB for some specific QW system. We do not discuss this issue in detail in this work.

It is well known that in the case of the total reflection geometry [see Fig. 1(a)], formation of a standing-wave pattern affects substantially linear and nonlinear intersubband response [15,20,24]. It is reasonable to expect that formation of a standing-wave pattern should also affect IOB pictures. Namely, radiation intensity in a QW is determined by the QW position in the standing wave, in particular with regard to its antinode and node, whose pattern is set by $d_{\rm SPAC}$. If so, we should observe strong dependence of the reflectance and IOB pictures of the considered structure on $d_{\rm SPAC}$. Note that the most pronounced IOB picture does not necessarily require a QW to be located only at the maximum of $|E_z|^2$ (antinode) of the standing wave because the IOB requires a certain intensity interval. However, if the IOB occurs with a QW at an antinode, it surely requires the smallest $\tilde{I}_{\rm inc}$.

Results of our numerical simulations displayed in Fig. 4 confirm the vital effect of the standing-wave pattern on the IOB pictures for one-QW system. They show that for any reasonable thickness of the GaAs spacer layer the IOB pictures for the QW-HMC system with the given parameters fall into the area between (a very close vicinity of) line 1 and (a very close vicinity of) line 4 in Fig. 4. We observe periodicity in the response of the QW system with changing thickness of the spacer layer. IOB pictures for our system repeat themselves with the period of 3.792 μm for the GaAs spacer layer

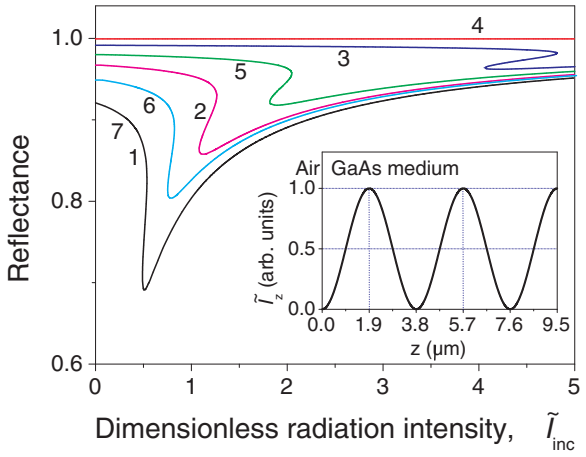

FIG. 4. (Color online) Dependence of reflectance on the dimensionless incident radiation intensity $\tilde{I}_{inc}$ for one-QW GaAs-QW-GaAs(d_{SPAC})-air structure with the same $d_B = 300$ Å for different thickness d_{SPAC} of the GaAs spacer layer: $d_{SPAC} = 1.9$ μm (1), $d_{SPAC} = 2.85$ μm (2), $d_{SPAC} = 3.3$ μm (3), $d_{SPAC} = 3.8$ μm (4), $d_{SPAC} = 4.3$ μm (5), $d_{SPAC} = 4.75$ μm (6), $d_{SPAC} = 5.692$ μm (7). Line 7 coincides with line 1. Period for d_{SPAC} is 3.792 μm. $\tilde{V}_{21} = 0.05$ and $N_S = 8\times10^{11}$ cm^{-2}. In the inset: standing-wave pattern of the normalized light intensity distribution (more precisely $|E_z|^2$), presented by $\sin^2(k_z z)$ function of the distance z with $k_z = (\omega/c)\sqrt{\varepsilon_{GaAs}}\cos\varphi$, in the homogeneous GaAs medium for $\varphi = 65^\circ$ that provides the total light reflection from the flat air-GaAs boundary at $z = 0$.

thickness. Lines 1 to 7 in Fig. 4 represent one period interval from 1.9 to 5.692 μm where the most pronounced IOB pictures occur at the edges of the interval and the least pronounced one exactly at the center of the interval. The IOB pictures for the thicknesses equidistant from the center of the interval are very different from each other.

To simplify analysis and assuming that influence of light reflection and absorption by the Q2DEG on the spatial variation of $\tilde{I}_z$ is small, we exploit the spatial distribution of light intensity in a plain GaAs homogeneous medium as a rough approximation for the intensity distribution in our multilayered QW system. In the inset of Fig. 4, we present the standing-wave pattern of the intensity distribution in the homogeneous (half-space) GaAs medium with a flat boundary with the air for the light propagating in the medium and reflecting from the boundary at the angle $\varphi = 65^\circ$ to provide the total reflection. The distance from the air-GaAs frontier to the QW position is well represented by d_{SPAC} when $d_B + d_{QW} \ll 2\pi/k_z$. Such a simplified plot of the intensity distribution greatly helps in understanding of the described peculiarities of the IOB pictures with regard to changing d_{SPAC}. In part, it illustrates the d_{SPAC}-period interval from 1.9 to 5.692 μm and the d_{SPAC} values for the most pronounced (line 1, when the QW is located at the 1.9-μm antinode) and the least pronounced (line 4, when the QW is at the 3.8-μm node) IOB pictures. [Note that GaAs-QW-GaAs (1.9 μm)-air and GaAs-QW-perfect metal structures with the same QW have the same standing-wave pattern.] Because the IOB requires an $\tilde{I}_{inc}$ interval, one can expect line 4 not to be a flat line. Our simulations show that although line 4 stands for the case of practically unchangeable total reflectance, it also features an IOB picture, like in the inset of Fig. 6, that occurs at about $\tilde{I}_{inc} = 60$ with the depth of switch about 0.999–0.997. The IOB pictures for the d_{SPAC} values equidistant from 3.8 μm are different due to the fact that the IOB requires different $\tilde{I}_{inc}$ intervals at those d_{SPAC} as is well illustrated by the inset in Fig. 4.

Our simulations show that IOB pictures for the interval 1.6–1.9 μm of the GaAs spacer layer thickness are not noticeably different from each other and are all well represented by line 1. We have also found that the IOB pictures do not noticeably change when the barrier width changes in the interval from 0 to 5000 Å.

2. *Two-QW-HMC system*

Now, we consider MQW-HMCs containing two identical QWs separated by different distances. Due to (i) formation of a standing-wave pattern and (ii) light reflection and absorption by the Q2DEG, the light intensity in the region occupied by the the first QW (the QW neighboring the spacer layer) is, in general, different from the light intensity in the region occupied by the second QW. In the following, we discuss influence of such spatial inhomogeneity of the light intensity (the spatial effect) in the QW-QW-HMC on the IOB response of the system. Figures 5 and 8 show that due to the spatial effect, OB pictures strongly depend on the separation between QWs (or, equivalently, on the barrier width d_B at a constant QW width).

At $d_B = 3000$ Å, the IOB picture in Fig. 5(a) is straightforward: two interconnected S-like curves which we call a double-S-like curve. Each individual S-like curve of the double-S-like curve represents the IOB process in one of the two QWs. However, a suggestion that the individual S-like curves are independent is erroneous. Actually, it is one integrated IOB process in the two-QW system that has one entrance at the lower intensity (for the forward process) and one exit at the higher intensity of the incident radiation. The exit of one S-like curve becomes the entrance of the other S-like curve. A reader may have a question: Is the number of S-like curves in an IOB picture for a MQW structure supposed to be always equal to the number of QWs in the structure?

It is very illustrative to compare the IOB picture for a system of two identical QWs whose oscillator strengths are equal to one with the IOB picture for a system of one "effective" QW whose oscillator strength is equal to two instead of one, with the rest of parameters of the system remaining the same. Figure 5(a) demonstrates such comparison and well illustrates that the IOB process in QW-QW-HMC is an integrated process of the entire system and not of individual and separate QWs. From the comparison, one can see that for a system of two identical QWs the parts of the IOB picture everywhere except the area of the double-S-like curves practically coincide with the corresponding parts of the IOB picture for one "effective" QW whose oscillator strength is equal to the sum of the oscillator strengths over all the QWs in the two-QW system. Our simulations show that it holds true for d_B up to about 5000 Å.

Is that the case for any system of more than two identical QWs? Our calculations for systems of a few QWs show

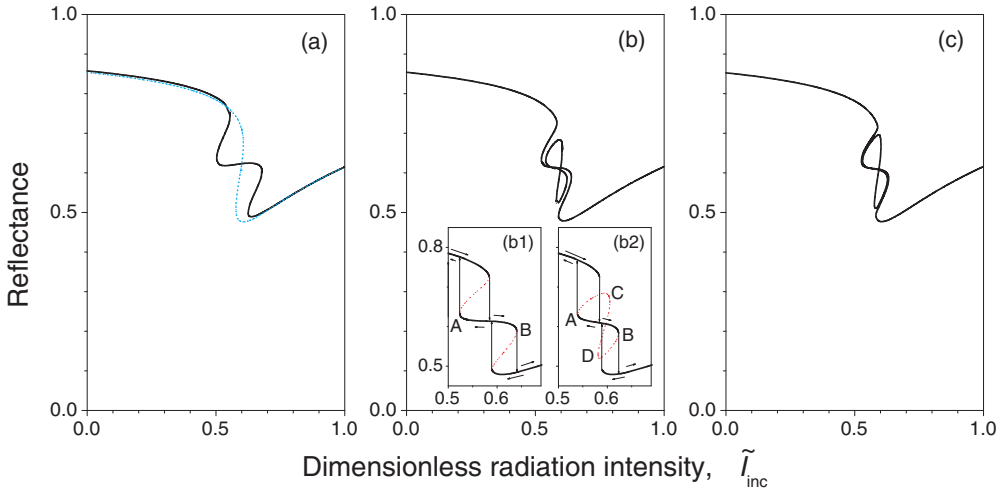

FIG. 5. (Color online) Dependence of reflectance on the dimensionless incident radiation intensity $\tilde{I}_{inc}$ for two-QW GaAs-MQW-GaAs(1.9 μm)-air structure for different barrier thickness d_B: $d_B = 3000$ Å (a), $d_B = 1000$ Å (b), $d_B = 300$ Å (c). Dotted line in (a) represents one QW with the oscillator strength equal to 2. Insets in (b) show possible discontinuous transitions for the IOBR process in (b). Period for d_B is 51 770 Å. $\tilde{V}_{21} = 0.05$ and $N_S = 8\times10^{11}$ cm^{-2}.

that the answer can be positive, provided that the "effective" barrier thickness for one "effective" QW with the summed oscillator strength is taken to be around the summed thickness of all barriers in the MQW system and the "effective" QW is symmetrically positioned between two "effective" barriers. It is because the IOB picture depends on the number of interfaces reflecting radiation and the distance between the interfaces.

For smaller d_B [Figs. 5(b) and 5(c)], the two-QW system features a complicated OB process presented by a combination of a double-S-like curve and an 8-like curve. All the double-S-like and 8-like curves in Figs. 5(b) and 5(c) look rather symmetric. A small difference between parameters of two QWs can make the picture very asymmetric. Note that assumption of the same dielectric constant 10.89 throughout the entire system ($\varepsilon_w = \varepsilon_b$) results in minor modification of the OB pictures in all panels in Fig. 5 that can practically be ignored. It means that due to a small difference between ε_w and ε_b, the effects associated with light reflection at the QW-barrier interfaces are negligible.

Let us discuss why the OB picture in Fig. 5 modifies so radically when the barrier thickness considerably decreases. Keeping in mind that a decrease of d_B is actually a decrease of the separation between sheets of the Q2DEG, a reader may ask if the effect is due to an increase of the interwell *e-e* interaction. Our estimations show that in the case of the considered system, when $\tilde{V}_{21}$ is taken constant and independent of d_B, we can safely assume that the interaction is not responsible for the modification of the OB pictures from Fig. 5(a) to Fig. 5(b) and to Fig. 5(c) when d_B decreases. (The role of the interwell *e-e* interaction in the IOB process in systems containing a large number of QWs will be considered in another paper.)

Then, one has to come to the conclusion that the appearance of a non-S-like curve in addition to a double-S-like curve in the OB picture manifests that radiation reflection at the interfaces essentially contributes to the complicated OB process that originates with a pure IOB. Our calculations show no OB in the considered system when the IOB is turned off ($V_{12} = 0$). Therefore, although 8-like curves and any other non-S-like curves feature properties of the MOB, once these non-S-like curves do not appear without double-S-like curves we do not say that they represent pure MOB processes in the considered cases. We do not call it a hybrid of the IOB and MOB either. We coin the name for it IOBR where "R" stands for the particular reflection contribution to the process of IOB. It should be stressed that reflection always affects the IOB process in layered systems, but IOBR pictures differ from pure IOB pictures by featuring non-S-like curves in addition to double-S-like curves. A non-S-like curve never associates with a single S-like curve for one-QW system. We model one QW by means of a sheet of Q2DEG. It is one sheet of Q2DEG that triggers the IOB. It is two sheets of Q2DEG that play a vital role as interfaces in formation of the IOBR pictures.

A key interface of our GaAs-MQWs-GaAs-air system that is involved in producing IOB and IOBR pictures is the GaAs-air interface. Therefore, as one can reasonably expect the thickness d_{SPAC} of the GaAs spacer layer that determines the position of the first QW with respect to the standing-wave pattern plays a crucial role for the whole IOBR process. Figure 6 demonstrates that the entire OB picture radically changes with changing d_{SPAC} while the barrier thickness stays the same $d_B = 300$ Å. It is helpful for analysis to refer to the simplified plot of the standing-wave pattern in the inset of Fig. 4 although the two-QW system modifies that pattern more than the one-QW system. First of all, we find that the IOB pictures repeat themselves when d_{SPAC} changes with the period of 3.792 μm. A reader can see that line 1 in Fig. 6 for $d_{SPAC} = 3.7$ μm that stands for practically 100% reflection of the incident radiation occurs when, due to small d_B, both QWs are located very close to the node of the standing-wave pattern. As the inset in Fig. 6 shows the two-QW system still features the IOB represented by one S-like curve with a vanishing depth of switch and the $\tilde{I}_{inc}$ threshold of around 300. When at $d_{SPAC} = 4$ μm the QWs are slightly distanced from the node the system features a pure well-distinguished double-S-like curve of the IOB with a small depth of switch and the $\tilde{I}_{inc}$ threshold of around 5.5. When d_{SPAC} grows further,

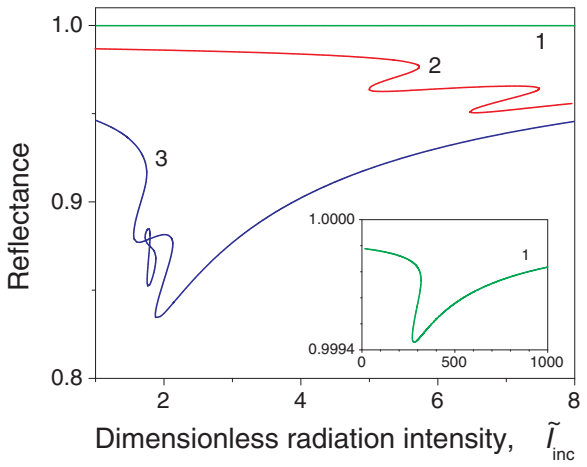

FIG. 6. (Color online) Dependence of reflectance on the dimensionless incident radiation intensity $\tilde{I}_{inc}$ for two-QW GaAs-MQW-GaAs(d_{SPAC})-air structure with the same barrier thickness $d_B = 300$ Å for different thickness d_{SPAC} of the GaAs spacer layer: $d_{SPAC} = 3.7$ μm (1), $d_{SPAC} = 4$ μm (2), and $d_{SPAC} = 4.3$ μm (3). Period for d_{SPAC} is 3.792 μm. $\tilde{V}_{21} = 0.05$ and $N_S = 8\times10^{11}$ cm^{-2}. The inset contains details on line 1.

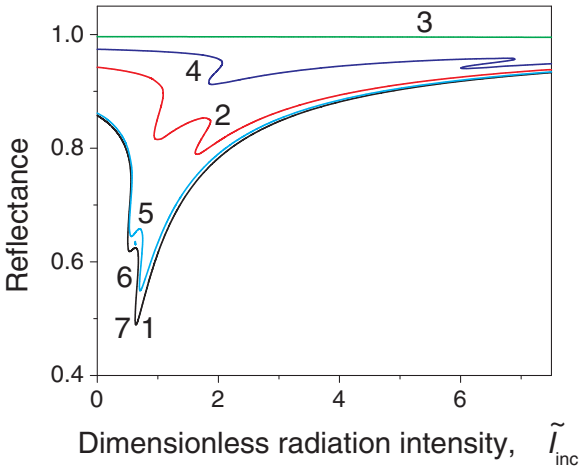

FIG. 7. (Color online) Dependence of reflectance on the dimensionless incident radiation intensity $\tilde{I}_{inc}$ for two-QW structure GaAs-MQW-GaAs(d_{SPAC})-air with the same $d_B = 3000$ Å for different thickness d_{SPAC} of the spacer layer GaAs: $d_{SPAC} = 1.9$ μm (1), $d_{SPAC} = 2.6$ μm (2), $d_{SPAC} = 3.2$ μm (3), $d_{SPAC} = 3.8$ μm (4), $d_{SPAC} = 4.878$ μm (5), $d_{SPAC} = 5.662$ μm (6), and $d_{SPAC} = 5.692$ μm (7). The double-S-like curve of line 6 practically coincides with line 7. Lines 7 and 1 coincide. Period for d_{SPAC} is 3.792 μm. $\tilde{V}_{21} = 0.05$ and $N_S = 8\times10^{11}$ cm^{-2}.

the $\tilde{I}_{inc}$ threshold for the IOB decreases. At $d_{SPAC} = 4.3$ μm, the system manifests a distinct 8-like curve and a double-S-like curve interwoven in a IOBR picture with a bigger depth of switch. Our simulations show that an IOBR picture emerges for d_{SPAC} being around 4.1 μm when a very small closed curve appears apart from a double-S-like curve.

Now, we take the two-QW GaAs-MQW-GaAs(d_{SPAC})-air structure with $d_B = 3000$ Å. The period for d_{SPAC} to repeat the OB pictures remains 3.792μm. We inspect how IOB pictures modify when d_{SPAC} changes on the one-period interval from 1.9 to 5.692 μm. In particular, we are interested to answer the following question: Does an IOBR picture appear for any d_{SPAC} for d_B much bigger than 300 Å? Figure 7 illustrates that a double-S-like curve is present in pictures at any d_{SPAC} except at $d_{SPAC} = 3.2$ μm (line 3) when a single S-like curve is observed with the depth of switch of about 0.99–0.98 at the intensity around 10. Line 3 represents the least pronounced IOB picture when the second QW that is farther from the GaAs spacer layer is practically located at the node of the standing-wave pattern while the first QW is rather distant from the node and thus features one S-like curve. Figure 7 shows a particular d_{SPAC} interval from 4.878 μm (line 5) to 5.662 μm (line 6) where the two-QW system features IOBR pictures. A reader can estimate that at those d_{SPAC} the QWs are located in the vicinity of the antidote of the standing-wave pattern. In the middle of the IOBR interval, the pictures look like those in Figs. 5(b) and 5(c). The double-S-like curve of line 6 practically coincides with lines 7 and 1. Thus, on the majority of the one-period interval for d_{SPAC}, the two-QW system features pure IOB pictures with smaller depth of switch and bigger $\tilde{I}_{inc}$ threshold. About 20% of the one-period interval is an IOBR interval with the deepest switch and the smallest $\tilde{I}_{inc}$ threshold.

Our simulations demonstrate that OB pictures for the considered QW-QW-HMC systems, no matter if they are IOB or IOBR pictures or any other pictures, repeat themselves with the period of 3.792 μm for changing thickness of the GaAs spacer layer at the barrier thickness of up to 5000 Å. The period for d_{SPAC} is the same 3.792 μm as for the one-QW and for the two-QW structure. The period becomes 3.8 μm when dielectric constants of the QW material and the barrier material are assumed to be the same 10.89. Note that the period of 3.8 μm works well for one-QW-HMC even with different dielectric constants, but it does not work so well for two-QW-HMC systems.

Taking into account that the $Al_{0.33}Ga_{0.67}As$ barrier between two QWs functions as a spacer layer, it is reasonable to check how IOB and IOBR pictures change with changing d_B. To distinguish the spacer layers, we call them a barrier spacer (with thickness d_B) and a frontier spacer with spacer-air frontier (with thickness d_{SPAC}). Is there a period for d_B as it is for d_{SPAC} when the pictures repeat themselves? Is there a value for d_B at which the IOB picture transforms into a practically flat line with 100% reflectance? We choose constant $d_{SPAC} = 1.9$ μm to conveniently locate the boundary between the GaAs spacer layer and the first AlGaAs barrier at the antinode of the standing-wave pattern (see the inset in Fig. 4).

Figure 8 illustrates the answers to those questions. There is a period of 5.177 μm for d_B of the AlGaAs barrier that is different form the period of 3.792 μm for d_{SPAC} of the GaAs spacer layer. For analysis, we can still exploit the plot of the standing-wave pattern but essential correction in determining the QWs location in the pattern is required. Now, the QW location is determined by both d_{SPAC} of GaAs and d_B of AlGaAs. We want to replace the AlGaAs barrier layer of d_B thickness by an effective GaAs layer of d_B^* thickness to provide as close as possible a standing-wave pattern. Then, we can use the plot of the standing-wave pattern for the homogeneous GaAs medium. Since $d_{QW} = 90$ Å is much

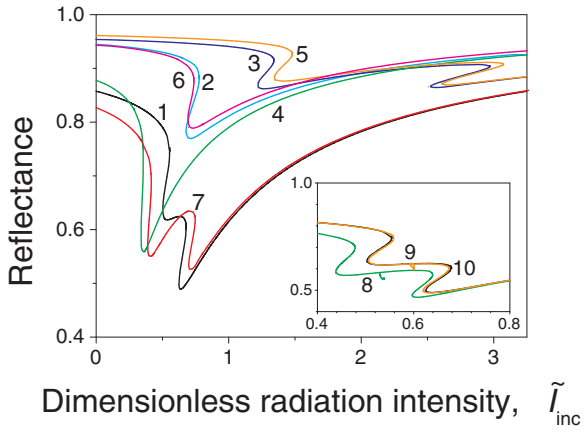

FIG. 8. (Color online) Dependence of reflectance on the dimensionless incident radiation intensity $\tilde{I}_{inc}$ for two-QW structure GaAs-MQW-GaAs(1.9 μm)-air for different barrier thickness d_B : d_B = 0.3 μm (1), d_B = 1.1 μm (2), d_B = 1.73 μm (3), d_B = 2.5 μm (4), d_B = 3.47 μm (5), d_B = 3.8 μm (6), d_B = 4.5 μm (7), d_B = 4.7 μm (8), d_B = 5.457 μm (9), and d_B = 5.477 μm (10). The double-S-like curve of line 9 practically coincides with line 10. Lines 10 and 1 coincide. Period for d_B is 5.177 μm. $\tilde{V}_{21} = 0.05$ and $N_S = 8\times10^{11}$ cm^{-2}.

smaller than d_{SPAC} and d_B, we can consider the whole two-QW system as a homogeneous AlGaAs layer whose thickness is $2d_B$. By zeroing the optical path difference for the AlGaAs and GaAs media and taking into account the Snell's law for the 65° angle of incidence, we find that $d_B^*/d_B = 0.7657$. The ratio rather well explains the difference between 3.792- and 5.117-μm periods for GaAs and AlGaAs, respectively. However, 3.792/5.117 = 0.733 differs from 0.7657 because the two-QW system differs from a homogeneous AlGaAs layer. We use 0.733. The real GaAs QW is surrounded at each side by the AlGaAs barrier of $d_B/2$ width. Such a multimedia structure is rendered into an effective pure GaAs medium layer when the GaAs QW has the effective GaAs barrier of d_B^* width at its one side that is closer to the GaAs spacer layer. So made effective pure GaAs QW systems provide standing-wave patterns and IOB pictures that are rather equivalent to those of the original QW systems. Now, the position of the first and the second QWs on the plot in the inset of Fig. 4 can be estimated as located at $z = d_{SPAC} + d_B^*$ and $z = d_{SPAC} + 2d_B^*$, respectively. A reader can see that line 1 with $d_B^* = 0.22$ μm in Fig. 8 represents two QWs located close to each other near the antinode at 1.9 μm that provides a very distinct double-S-like curve with a deep switch and a small $\tilde{I}_{inc}$ threshold. For line 2, $d_B^* = 0.81$ μm that locates the second QW very close to the 3.8-μm node with relative intensity of 0.05 in the QW while the relative intensity at the first QW is 0.61. Thus, line 2 is practically a single S-like curve manifested by the first QW with the depth of switch quite smaller and $\tilde{I}_{inc}$ threshold bigger than for line 1. Similar to line 2 is line 6 with $d_B^* = 2.79$ μm when the second QW is very close to the 7.6-μm node and the single S-like curve is due to the first QW. Lines 3 and 5 have $d_B^* = 1.27$ μm and $d_B^* = 2.54$ μm, respectively, that position two QWs rather distant from the nodes although pretty distant from the antinodes as well. As a result, lines 3 and 5 are double-S-like curves with the smallest depth of switch, the biggest $\tilde{I}_{inc}$ threshold, and with the individual S-like curves being rather distant from each other on the $\tilde{I}_{inc}$ scale. Line 4 with $d_B^* = 1.83$ μm features a very special case when the first QW is located practically at the 3.8-μm node while the second QW is practically at the 5.7-μm antinode. Line 4 presents a very distinct single S-like curve with the deepest switch and the smallest $\tilde{I}_{inc}$ threshold provided by the second QW. Line 7 with $d_B^* = 3.45$ μm has the relative intensities 0.92 and 0.62 in the first and second QWs, respectively, that explains a very deep switch of the S-like curve for the first QW and a smaller depth of switch for the second QW. Lines 8, 9, and 10 have the QWs located in the proximity of the antinodes at 5.7 and 9.5 μm with the relative intensity of about 0.9 in each QW that pretty much explains the features of those three lines. Lines 8 and 9 mark the 0.757-μm-long IOBR interval for d_B. The IOBR pictures in the middle of that interval are presented in Figs. 5(b) and 5(c) for small d_B due to the d_B periodicity.

Thus, our approach to replace the spatial intensity distribution in the considered nonhomogeneous two-QW systems with the intensity distribution in an effective homogeneous medium allows us to qualitatively describe and roughly quantitatively evaluate modification of the obtained IOB pictures in Fig. 8 when d_B changes at constant d_{SPAC}. In addition, it answers that there can never be a d_B that transforms an IOB picture into a practically flat 100% reflectance line for $d_{SPAC} = 1.9$ μm. It is definitely possible for d_{SPAC} close to 3.8 μm. In addition, the approach explains that due to the periodicity of the standing-wave pattern, the 5.177-μm-long one-period interval for d_B has three almost equal intervals marked by 1.73 and 3.47 μm that correspond to lines 3 and 5, respectively, with the smallest depth of switch. Moreover, in each of the two intervals, there are d_B that provide IOB pictures with a single S-like curve (lines 2 and 6). The approach shows that approximately in the middle of the one-period d_B interval (line 4), one QW is located very close to the antinode while the other is very close to the node. Besides, it demonstrates that at those d_B when OB pictures with double-S-like curves are the most pronounced, there is an interval where the two-QW system features IOBR pictures. The IOBR interval is about 15% of the one-period interval. Those are the general features of the IOB pictures on the one-period interval for d_B.

Inspecting the figures, we can suggest that the IOBR picture occurs in a two-QW system when the radiation intensities in two QWs are quite close to each other. It is usually observed for two QWs located close to each other in the vicinity of antinodes when $\tilde{I}_{inc}$ threshold is very small (see lines 8 and 9 in Fig. 8). When the intensities in two QWs differ essentially from each other, the system does not feature the IOBR, but a pure IOB picture with double-S-like curve (line 7). We have found it useful to introduce two ratios $\mathcal{F}_S$ and $\mathcal{F}_{\nu\nu'}$ to determine the condition for the IOBR. We define $\mathcal{F}_S = 2|\tilde{I}_z^{max} - \tilde{I}_z^{min}|/|\tilde{I}_z^{max} + \tilde{I}_z^{min}|$ to represent the relative IOB interval for $\tilde{I}_z$ where the cubic equation (9) has three different real roots. The inset in Fig. 2(c) shows that $\mathcal{F}_S \approx 0.081$ for the considered QW. $\mathcal{F}_{\nu\nu'} = 2|\tilde{I}_z^{\nu} - \tilde{I}_z^{\nu'}|/|\tilde{I}_z^{\nu} + \tilde{I}_z^{\nu'}|$ stands for the relative difference between values of $\tilde{I}_z$ from the middle of the IOB intervals in the νth and ν'th QWs. Values for $\tilde{I}_z^{\nu}$ and $\tilde{I}_z^{\nu'}$ can be estimated by means of the standing-wave pattern for given d_{SPAC} and d_B. We suggest the following condition for

the IOBR:

$$\mathcal{F}_{\nu\nu'} \leqslant \mathcal{F}_S. \tag{21}$$

The condition for practical IOBR pictures is the easiest to meet for two QWs located in the vicinity of the antinodes. A reader can readily check with the inset in Fig. 4 that in a two-QW system with $d_{\mathrm{SPAC}} = 1.9$ μm and one QW located exactly at the antinode distinguished IOBR pictures require $d_{\mathrm{B}} < 2300$ Å according to $\mathcal{F}_{12} \leqslant 0.081$, which is confirmed by our simulations. It also explains the 15% IOBR interval on the one-period interval for d_{B}. Our simulations show that two QWs placed in the proximity of the node with vanishing d_{B} and d_{QW} also produce an IOBR picture but with 0.999–0.998 depth of switch and the $\tilde{I}_{\mathrm{inc}}$ threshold of around 170.

3. *Many-QW-HMC system*

From a practical point of view, clear and straightforward IOB pictures may look more preferable than complicated and confusing IOBR pictures. Pure IOB pictures in MQW structures require a certain thickness for barrier and spacer layer. Bearing that in mind, we consider MQW-HMC systems with three [Fig. 9(a)], five [Fig. 9(b)], and ten [Fig. 9(c)] QWs taking $d_{\mathrm{B}} = 3000$ Å to provide pure and deep IOB pictures for $d_{\mathrm{SPAC}} = 1.9$ μm.

To explain the features of the IOB pictures observed in Fig. 9, we apply the simplified approach developed in the previous section to locate each QW in the standing-wave pattern shown in the inset of Fig. 4. Let us consider ten QWs. One can estimate that for $d_{\mathrm{B}}^{*} = 0.22$ μm that corresponds to $d_{\mathrm{B}} = 3000$ Å the first nine QWs are located equidistantly from the 1.9-μm antinode to the 3.8-μm node. The eighth and ninth QWs are located in the very close vicinity of the node. It means that in the series of nine QWs, each QW to feature the IOB requires a bigger $\tilde{I}_{\mathrm{inc}}$ than the previous QW. Besides, the depth of switch decreases for each next QW. Only in the first four QWs, the relative intensity is bigger than 0.5. It well explains the IOB pictures displayed in Fig. 9, in part why the first four QWs feature more distinct S-like curves than the other QWs and why the IOB picture for the eighth QW is hardly seen and for the ninth QW practically undetectable at rather big $\tilde{I}_{\mathrm{inc}}$. In addition, it explains why with growing $\tilde{I}_{\mathrm{inc}}$ the reflectance decreases until $\tilde{I}_{\mathrm{inc}} < 1$ when the IOB is featured by the first three QWs and increases for $\tilde{I}_{\mathrm{inc}} > 1$ when the fourth and other QWs manifest the IOB. The reason is that for $\tilde{I}_{\mathrm{inc}} > 1$, the first three QWs quit the resonant IOB area that makes reflectance rapidly rising with growing $\tilde{I}_{\mathrm{inc}}$. Note that at $\tilde{I}_{\mathrm{inc}} = 15$ in Fig. 9(c) all QWs still have $\triangle\rho_{12} < 0.4$. What about the tenth QW? Its location on the intensity distribution plot, being rather distant from the node, shows that it manifests the IOB after the seventh QW when $\tilde{I}_{\mathrm{inc}}$ gains the value appropriate for it.

What do the IOB pictures look like for MQW with bigger numbers of QWs? Using the intensity distribution plot, we estimate the values of $\tilde{I}_z$ in each QW and arrange them in a descending series. In other words, we map all QWs on the 1.9–3.8 branch of the plot according to their values of $\tilde{I}_z$. When $\tilde{I}_{\mathrm{inc}}$ grows from zero for the forward IOB process and $\tilde{I}_z$ goes, correspondingly, from 1 to zero, the QWs successively enter the IOB regime. One can reasonably expect that when the number of QWs is very big, the $\tilde{I}_z$ intervals required for the IOB in different QWs can overlap, which would make the OB picture for the whole MQW very complicated. Our simulations show that IOB pictures for MQW with dozens of QWs still generally look like the one in Fig. 9(c). Besides, for a bigger number of QWs, complicated IOBR pictures are observed with small depth of switch for individual switches and the reflection becomes close to nothing for a rather wide interval of incident radiation intensity.

Nonetheless, one can clearly see that only MQW with up to five QWs (for $d_{\mathrm{B}} = 3000$ Å) look practically applicable. It seems quite possible to operate one or a few S-like curves by choice. For example, according to Fig. 9(b), when the IOB regime is entered it is possible to choose suitable incident radiation intensity intervals to execute one through five switches on the chosen S-like curves. Does this sound like a possibility of functional realization of multistability?

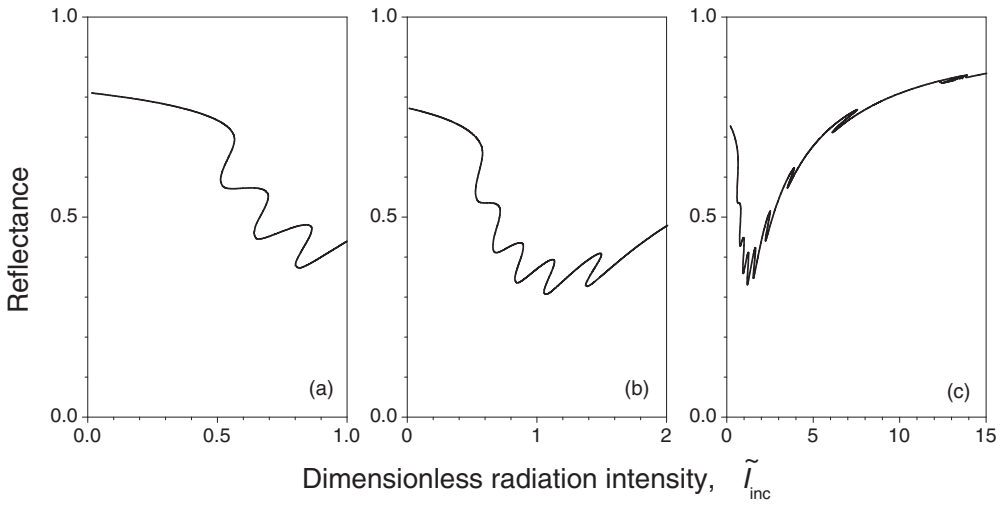

FIG. 9. Dependence of reflectance on the dimensionless incident radiation intensity $\tilde{I}_{\mathrm{inc}}$ for different numbers of QWs in GaAs-MQW-GaAs(1.9 μm)-air structure: three QWs (a), five QWs (b), and ten QWs (c). Period for AlGaAs barrier thickness is 5.177 μm. Period for GaAs spacer layer thickness is 3.792 μm. $d_{\mathrm{B}} = 3000$ Å, $\tilde{V}_{21} = 0.05$, and $N_{\mathrm{S}} = 8\times10^{11}$ cm^{-2}.

A reader can suggest that in a MQW with many QWs with $d_B^* = 1.9\ \mu$m ($d_B = 2.59\ \mu$m), only the even QWs that are all located at the antinodes would feature distinct S-like curves in only one interval of small $\tilde{I}_{inc}$ because all odd QWs are located at the nodes. In addition, one can suggest a considerable increase of the depth of switch due to a cumulative effect of the same IOB process in each even QW. It works that way to some extent. However, the combined OB process displays a complicated IOBR picture with a growing number of QWs. One should acknowledge that the suggestion is based on the assumption that the simplified plot of the standing-wave pattern in MQW firmly holds true, which is not exactly true. On top of that, the IOB process always requires an intensity interval which can be different for different QWs, which complicates the picture.

Now, we address the question if the number of S-like curves on IOB pictures is equal to the number of QWs. As the displayed figures demonstrate, the number of QWs determines the maximum possible number of well-distinguished S-like curves. For MQW with a few QWs at a certain thickness of the barrier and spacer layer, the number of well-distinguished S-like curves can be smaller than the maximum (see Fig. 8). A special case is for systems with big numbers of QWs when only a handful of QWs can feature distinct S-like curves.

Note that Figs. 5 and 9 would look differently for different values of $\hbar\omega$ and φ. Besides, when the number of QWs is rather big, a picture like in Fig. 5(b) can occur at smaller incident intensity even for $d_B = 3000$ Å.

Some remarks about S-like curves in OB pictures. We assign an S-like curve to a pure IOB process. On the other hand, an S-like curve can as well represent a pure MOB in QW systems with MC. If in our calculations we deal with an S-like curve we know whether it represents a pure IOB or a pure MOB by the number of real roots of Eq. (9): if there are three real roots, we deal with the IOB for sure. How can one tell the difference when observing an S-like curve in experiment? That is a good question.

B. MQW-MC system

Although the OB phenomenon in MC (the presence of a coupling mirror) seems to be MOB by definition, the pure MOB is beyond the scope of this work. (The MOB in MQW was discussed in Ref. [18] where the depolarization effect was neglected, i.e., assuming $V_{21} = 0$.) Our focus is the IOB for MQW in MC. Having gotten acquainted in the previous subsection with the IOB features of MQW-HMC systems, now we are going to investigate how MC can influence those features when QW systems are located in MC [see Fig. 1(b)]. MC is thought to be employed mainly to reduce the incident light intensity required to provide the IOB and/or to optimize the bistable response. Knowing exactly how it can work is critical for practical operation.

Contrary to the HMC layered structures, the MC influence on MQW is based on the resonance enhancement and formation of the eigenmodes of the light inside the cavity due to light reflection from the MC mirror (and from all the structure's interfaces). Strength of the resonant enhancement of the light in MC is controlled by the transmissivity of the coupling mirror which depends on the mirror layer thickness (d_{MIRR}). An MC eigenmode coupled resonantly to the incident light of a given frequency ω and a given angle of incidence φ is formed at a certain separation between the cavity mirrors. Light intensity at the antinodes of the eigenmode is much bigger than for a nonresonant case. Thus, the IOB regime can require a much smaller $\tilde{I}_{inc}$ threshold when the MC eigenmodes are employed. In the following figures, we present the energy of the nth MC eigenmode $\hbar\omega_{MC}^{(n)}$, that is the closest to $\hbar\omega$ of the incident light for the given MQW-MC structures and $\varphi = 65^\circ$, where n stands for the number of antinodes in MC. When $\hbar\omega_{MC}^{(n)}$ is very close to $\hbar\omega$ (the resonant coupling regime), it means that big $\tilde{I}_z$ in a QW can be reached at small $\tilde{I}_{inc}$. By manipulation of thickness of each layer of MQW-MC we can engineer as the overall spatial light intensity distribution in the structure as the light intensity in a specific QW. That way, we can directly affect $\triangle\rho_{12}(\tilde{I}_{inc})$ and, thus, the IOB produced by the conductivity. However, the overall picture is also determined by $\mathcal{R}_z^{(\mathcal{N})}$ in Eq. (20).

1. One-QW-MC system

We choose GaAs-AlAs-MQW-$Al_{0.33}Ga_{0.67}As$ − air structure to be a MQW-MC system where AlAs layer functions as the coupling mirror and $Al_{0.33}Ga_{0.67}As$ as the spacer before the $Al_{0.33}Ga_{0.67}As$-air boundary that functions as another mirror [Fig. 1(b)]. We start with one QW in the MC with changing d_{SPAC} at constant $d_{MIRR} = 2.6\ \mu$m and $d_B = 300$ Å.

Figure 10 demonstrates remarkable modifications of the IOB picture when d_{SPAC} changes. The IOB picture is the most pronounced at $d_{SPAC} = 3.85\ \mu$m and it practically

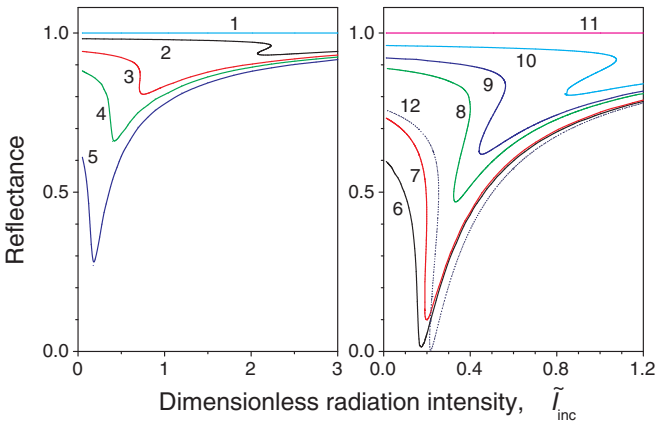

FIG. 10. (Color online) Dependence of reflectance on the dimensionless incident radiation intensity $\tilde{I}_{inc}$ for one-QW GaAs-AlAs(2.6 μm)-QW-AlGaAs(d_{SPAC})-air structure with the same $d_B =$ 300 Å for different thickness d_{SPAC} of the spacer-layer AlGaAs with the corresponding MC eigenenergy $\hbar\omega_{MC}^{(n)}$: $d_{SPAC} = 0\ \mu$m (1), $d_{SPAC} = 2.6\ \mu$m, $\hbar\omega_{MC}^{(1)} = 168.5$ meV (2), $d_{SPAC} = 3.2\ \mu$m, $\hbar\omega_{MC}^{(1)} = 138.1$ meV (3), $d_{SPAC} = 3.4\ \mu$m, $\hbar\omega_{MC}^{(1)} = 130.3$ meV (4), $d_{SPAC} = 3.6\ \mu$m, $\hbar\omega_{MC}^{(1)} = 123.3$ meV (5), $d_{SPAC} = 3.8\ \mu$m, $\hbar\omega_{MC}^{(1)} = 117.1$ meV (6), $d_{SPAC} = 3.85\ \mu$m, $\hbar\omega_{MC}^{(1)} = 115.6$ meV (7), $d_{SPAC} = 3.95\ \mu$m, $\hbar\omega_{MC}^{(1)} = 112.8$ meV (8), $d_{SPAC} = 4.0\ \mu$m, $\hbar\omega_{MC}^{(1)} = 111.5$ meV (9), $d_{SPAC} = 4.1\ \mu$m, $\hbar\omega_{MC}^{(1)} = 108.9$ meV (10), and $d_{SPAC} = 5.1\ \mu$m, $\hbar\omega_{MC}^{(1)} = 88.4$ meV (11). Line 12 represents QW-MC with $d_{MIRR} = d_{SPAC} = 3.8\ \mu$m and $\hbar\omega_{MC}^{(1)} = 116.6$ meV. Period for d_{SPAC} is 5.175 μm. $\hbar\omega = 117.2$ meV. $\tilde{V}_{21} = 0.05$, and $N_S = 8\times10^{11}$ cm^{-2}.

vanishes at $d_{\mathrm{SPAC}} = 0$ and 5.1μm. (Note that lines 1 and 11 feature practically undetectable IOB picture with the depth of 0.9999–0.9997 at the intensity of about 10 000 similar to that in the inset in Fig. 6.) IOB pictures repeat themselves when d_{SPAC} changes with the period of 5.175 μm that is associated with the periodicity of the MC eigenmodes. Figure 10 represents a change of the IOB pictures on the first period of d_{SPAC} from 0 to 5.1μm. The IOB pictures are not symmetrically located on the period interval and there are intervals of d_{SPAC} with no IOB, with hardly observed IOB, and with the most sound IOB.

The key to understanding these peculiarities is to see how close $\hbar\omega_{\mathrm{MC}}^{(n)}$ is to $\hbar\omega$. The most sound IOB picture with the smallest $\tilde{I}_{\mathrm{inc}}$ threshold, the deepest switch, and the reflectance close to zero occurs at $d_{\mathrm{SPAC}} = 3.85$ μm (which is not the center of the period interval). $\hbar\omega_{\mathrm{MC}}^{(1)} = 115.6$ meV is very close to 117.2 meV of $\hbar\omega$ that shows that the spatial distribution of intensity is very close to the ground MC eigenmode for the given ω. Although the QW is not exactly positioned at the antinode, the minimum value of the reflection reaches practically zero. The resonant enhancement of light in MC tremendously pronounces the IOB pictures in the d_{SPAC} interval of about 3.85–3.95 μm.

Note that when d_{SPAC} belongs to the intervals of about 3–3.2 μm and about 3.95–4.2 μm the IOB pictures for QW-MC are similar, by their depth of switch and the $\tilde{I}_{\mathrm{inc}}$ threshold, to those for QW-HMC that shows ineffectiveness of the MC for those intervals.

Line 6 for $d_{\mathrm{SPAC}} = 3.8$ μm represents the case when $\hbar\omega_{\mathrm{MC}}^{(1)} = 117.1$ meV practically equals $\hbar\omega = 117.2$ meV that unambiguously manifests formation of the MC eigenmode for the given ω with one antinode located around the middle of the MC. The reflection approaches practically zero as its minimum value at the smallest $\tilde{I}_{\mathrm{inc}} \approx 0.16$. However, line 6 does not feature an S-like curve. As one can see in Fig. 10, there is a whole d_{SPAC} interval of around 3.2–3.8 μm where the lines are not S like.

Does it mean that there is no IOB for that interval of d_{SPAC}? Comparing line 6 in Fig. 10 with line 2 in Fig. 2(a), the answer may seem to be positive at the first look. However, a deeper analysis questions that answer. All lines in Fig. 10 represent the same QW which is described by the same cubic equation (9) with the same parameters a, b, and c and the same solution $\Delta\rho_{12}(\tilde{I}_z)$ presented in the inset of Fig. 2(c). Our scrupulous analysis confirms that S-like lines in Fig. 10 represent the IOB. Therefore, all the lines in Fig. 10, including non-S-like lines 4, 5, and 6, have their intervals of $\tilde{I}_{\mathrm{inc}}$ where the cubic equation has three different real roots for $\Delta\rho_{12}$. An S-like dependence of $\Delta\rho_{12}(\tilde{I}_{\mathrm{inc}})$ is the heart of the IOB process when electron distribution between the subbands changes discontinuously under intense incident radiation. An S-like dependence of $\Delta\rho_{12}(\tilde{I}_{\mathrm{inc}})$ reveals an S-like dependence of the conductivity and other physical quantities that are derived from the conductivity. Without S-like dependence of $\Delta\rho_{12}(\tilde{I}_{\mathrm{inc}})$, there is no IOB. Thus, it seems to be safe to say that there is the IOB if there is an S-like dependence of $\Delta\rho_{12}(\tilde{I}_{\mathrm{inc}})$. By such a definition, all lines in Fig. 10 represent the IOB. Indeed, our simulations show that the same QW features an S-like curve for reflectance when the mirror thickness is smaller than about 1.5 μm and bigger than about 3.5 μm for the same $d_{\mathrm{SPAC}} = 3.8$ μm. In addition, two QWs with $d_{\mathrm{MIRR}} = 2.6$ μm, $d_{\mathrm{SPAC}} = 3.8$ μm, and $d_{\mathrm{B}} = 300$ Å manifest a pronounced IOBR picture similar to the one presented by line 1 in Fig. 12. If the QW did not feature the IOB process, it could not be produced by merely changing d_{MIRR} or by coupling QWs. On the other hand, lines 4, 5, and 6 are not S like, which is not typical for the IOB. If we call no IOB for lines 4, 5, and 6, it would mean that there is no S-like dependence for $\Delta\rho_{12}(\tilde{I}_{\mathrm{inc}})$ for them, which is not true. We call it a "hidden IOB" or "latent IOB" when an S-like dependence for $\Delta\rho_{12}(\tilde{I}_{\mathrm{inc}})$ does not reveal an S-like dependence of some other physical quantities that are derived from the conductivity. The hidden IOB in lines 4, 5, and 6 is an effect of the MC. The hidden IOB may seem to be a case of the IOBR for a single QW system in MC. We observe IOBR pictures for two and more QWs in MQW-HMC and MQW-MC when some additional closed lines appear near S-like curves. For the hidden IOB in one QW, an S-like curve transforms into a non-S-like curve due to the effect of radiation reflection from interfaces. Referring to Eq. (20), a reader can see that to produce a non-S-like line 6 an IOB S-like curve from the conductivity should be compensated by a counter S-like curve from MC that manifests the MOB. The MOB hides the IOB. Likewise, the IOB hides the MOB. Thus, it is equivalent to call it hidden IOB or hidden MOB because they are complementary to each other. In addition, it can be called hidden OB. We call it hidden IOB because we focus on the IOB.

MQW-MC structures are frequently manufactured with QWs located at the antinode of the spatial distribution of the radiation intensity that is at the center of the structure when $d_{\mathrm{MIRR}} = d_{\mathrm{SPAC}}$. Our simulations for structures with $d_{\mathrm{MIRR}} = d_{\mathrm{SPAC}}$ show that modification of the pictures for the reflectance dependence with growing d_{SPAC} generally resembles the one in Fig. 10 where d_{MIRR} is, however, fixed. In Fig. 10, lines 2 and 12 represent the structure with $d_{\mathrm{MIRR}} = d_{\mathrm{SPAC}}$ for 2.6 and 3.8 μm, respectively. A reader may suggest that the role of d_{SPAC} is major, while the role of d_{MIRR} is minor in production of OB pictures. Is it really so?

Figure 11 is very illustrative of the complicated effect of radiation reflection from interfaces in QW-MC. Three different QWs from Fig. 2(a) are chosen for comparison. Among three values 0.01, 0.04, and 0.05 for $\tilde{V}_{21}$, only 0.05 provides three different real roots for $\Delta\rho_{12}$ and therefore the IOB. By changing d_{MIRR} at constant $d_{\mathrm{SPAC}} = 3.8$ μm, we observe radical modification of the reflectance dependence. The QW structures with $\tilde{V}_{21} = 0.01$ and 0.04 that do not provide the IOB and are not expected to produce S-like curves (as it is with lines 1a, 1b, 2a, and 2b) manifest very pronounced S-like lines 1c and 2c in Fig. 11(c) that are represented by the ratio $\mathcal{R}_z^{(\mathcal{N})}$ in Eq. (20). The lines 1c and 2c represent a pure MOB process when a QW serves as a nonlinear element required to provide the positive feedback for the radiation reflection in the microcavity. The QW structure with $\tilde{V}_{21} = 0.05$ that provides the IOB and is expected to demonstrate an S-like curve for reflectance does not produce an S-like curve for some interval of d_{MIRR} in part in line 3b for 2.6 μm, thus featuring the hidden IOB. For $d_{\mathrm{MIRR}} = 4.8$ μm, the system manifests a profound combined IOB and MOB phenomenon by line 3c. Figure 11 demonstrates the challenge the OB phenomena in MQW MC present for investigation, in particular for the experiment when

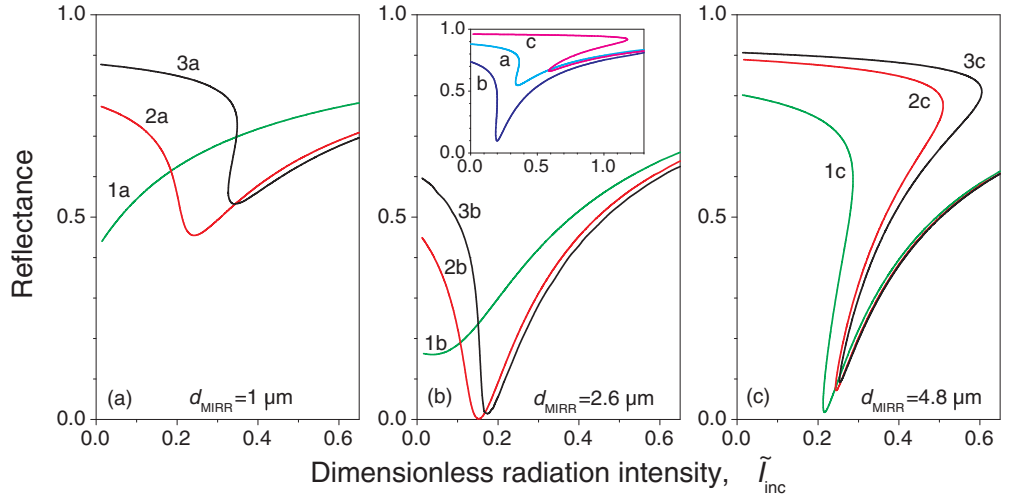

FIG. 11. (Color online) Dependence of reflectance on the dimensionless incident radiation intensity $\tilde{I}_{inc}$ for one-QW GaAs-AlAs(d_{MIRR})-QW-AlGaAs(3.8 μm)-air structure with the same $d_B = 300$ Å for different d_{MIRR} and different $\tilde{V}_{21}$: (1a) no OB for $\tilde{V}_{21} = 0.01$ and $d_{MIRR} = 1$ μm, (2a) no OB for $\tilde{V}_{21} = 0.04$ and $d_{MIRR} = 1$ μm, (3a) IOB for $\tilde{V}_{21} = 0.05$ and $d_{MIRR} = 1$ μm, (1b) no OB for $\tilde{V}_{21} = 0.01$ and $d_{MIRR} = 2.6$ μm, (2b) no OB for $\tilde{V}_{21} = 0.04$ and $d_{MIRR} = 2.6$ μm, (3b) hidden IOB for $\tilde{V}_{21} = 0.05$ and $d_{MIRR} = 2.6$ μm, (1c) MOB for $\tilde{V}_{21} = 0.01$ and $d_{MIRR} = 4.8$ μm, (2c) MOB for $\tilde{V}_{21} = 0.04$ for $d_{MIRR} = 4.8$ μm, and (3c) MOB+IOB for $\tilde{V}_{21} = 0.05$ and $d_{MIRR} = 4.8$ μm. $\hbar\omega^{(1)}_{MC}$ is 120.8, 117.1, and 116.5 meV for d_{MIRR} equaled to 1, 2.6, and 4.8 μm, respectively. In the inset: dependence of reflectance on $\tilde{I}_{inc}$ for one-QW GaAs-AlAs(d_{MIRR})-QW-AlGaAs(3.85 μm)-air structure with the same $d_B = 300$ Å and $\tilde{V}_{21} = 0.05$ for different d_{MIRR}: (a) IOB for $d_{MIRR} = 1$ μm and $\hbar\omega^{(1)}_{MC} = 119.5$ meV, (b) IOB for $d_{MIRR} = 2.6$ μm and $\hbar\omega^{(1)}_{MC} = 115.7$ meV, and (c) IOB+MOB for $d_{MIRR} = 4.8$ μm and $\hbar\omega^{(1)}_{MC} = 115$ meV.

the real OB process disguises and an appearance can be easily misinterpreted.

As Figs. 11(a) and 11(b) show, the reflectance increases with d_{MIRR} decreasing from 2.6 μm. When d_{MIRR} reaches 0.5 μm, the reflectance dependence for the QW-MC structure is practically the same as for the QW-HMC presented in Fig. 2(a). Further reduction of d_{MIRR} causes further increase of the reflectance.

In this work, we do not focus on the MOB which is always lurking around and will be addressed in a separate paper. Therefore, we choose $d_{SPAC} = 3.85$ μm to avoid the MOB and $d_{MIRR} = 2.6$ μm to provide the most pronounced IOB picture for $\tilde{V}_{21} = 0.05$. The inset in Fig. 11(b) illustrates that the IOB picture for $d_{SPAC} = 3.85$ μm and $\tilde{V}_{21} = 0.05$ becomes shallower and with a bigger $\tilde{I}_{inc}$ threshold for d_{MIRR} more distant from 2.6 μm. Although the IOB occurs at any d_{MIRR}, the combined OB process of IOB and MOB takes place for bigger d_{MIRR} as is represented by line c in the inset.

As Fig. 10 demonstrates, the most pronounced IOB picture for one QW with $d_B = 300$ Å in the GaAs-AlAs-QW-$Al_{0.33}Ga_{0.67}As$-air structure takes place for $d_{SPAC} = 3.85$ μm and $d_{MIRR} = 2.6$ μm. We would like to see how the IOB picture changes when the $Al_{0.33}Ga_{0.67}As$ spacer layer is replaced by the GaAs spacer layer in the GaAs-AlAs-QW-AlGaAs-air structure. Or, on the other hand, we would like to see how the IOB picture changes when the coupling mirror is incorporated in the GaAs-QW-GaAs-air structure used as a QW-HMC system in the previous section.

We consider GaAs-AlAs-QW-GaAs-air and GaAs-AlAs-GaAs-QW-GaAs-air structures with the same AlAs coupling mirror layer. It appears that with varying thickness of the GaAs spacer layer, IOB pictures of these two structures modify in a similar fashion as is illustrated in Fig. 10. We have found that for all the structures, the IOB pictures repeat themselves when thickness of any of the GaAs spacer layers changes with the period of 3.792 μm. The structure GaAs-AlAs-GaAs-QW-GaAs-air with two GaAs spacer layers features the same IOB pictures as the structure GaAs-AlAs-QW-GaAs-air with one GaAs spacer layer when certain thicknesses of the spacer layers are chosen. Moreover, one can choose a thickness of the equivalent GaAs spacer layer that gives an IOB picture which is very close to the IOB picture for a given thickness of the AlGaAs spacer layer. For example, line 7 in Fig. 10 is practically repeated by the IOB pictures of the following structures with the equivalent GaAs spacer layers: (1) GaAs-AlAs(2.6 μm)-GaAs(0.8 μm)-QW-GaAs(1.9 μm)-air with $\hbar\omega^{(1)}_{MC} = 114.9$ meV, (2) GaAs-AlAs(2.6 μm)-GaAs(3.792 μm)- QW-GaAs(2.68 μm)-air with $\hbar\omega^{(1)}_{MC} = 116.4$ meV, and (3) GaAs-AlAs(2.6 μm)-QW-GaAs(2.68 μm)-air with $\hbar\omega^{(1)}_{MC} = 115.4$ meV. The difference between the periods for the AlGaAs spacer layer (5.175 μm) and the GaAs spacer layer (3.792 μm) comes from the difference of the optical paths in the two media at the 65° angle of incidence (as is already discussed in Sec. IIIA2).

Inspecting line 1 in Fig. 4 for GaAs-QW-GaAs-air structure and line 7 in Fig. 10 that practically represents GaAs-AlAs-GaAs-QW-GaAs-air structure with the same thickness 1.9 μm of the frontier GaAs spacer layer, a reader can see that incorporation of the coupling mirror layer AlAs with an additional GaAs spacer layer can greatly increase the depth of switch and essentially reduce the $\tilde{I}_{inc}$ threshold for the IOB pictures.

2. *Two-QW-MC system*

Now, we deal with two identical QWs in MC. We choose GaAs-AlAs-MQW-$Al_{0.33}Ga_{0.67}As$-air structure with $d_{MIRR} = 2.6$ μm and $d_{SPAC} = 3.85$ μm. A new variable thickness parameter appears that represents the changing distance between two QWs. At a fixed QW width it is d_B. By changing d_B we modify the overall spatial distribution of intensity inside the MC, in particular, formation of the MC eigenmodes that we check by $\hbar\omega_{MC}^{(n)}$, as well as the position of each of the two QWs with regard to the antinodes and nodes of the intensity distribution. (Note that with the MQW-HMC systems we change practically only the position of each of two QWs in the spatial distribution of intensity which is a standing-wave pattern.)

We are interested in how IOB pictures change with varying barrier width starting with $d_B = 300$ Å. Figure 12 demonstrates that IOB pictures modify dramatically. At $d_B = 300$ Å, due to a very strong resonant enhancement of the light intensity in the QWs it is an IOBR picture which consists of two parts: (1) a typical double-S-like IOB curve and (2) a closed O-like curve. Note that smallness of d_B compared to the thickness of the MQW-MC system provides the light intensities in both QWs to be rather close to each other, which results in two distinctive effects: (i) each of the two QWs features an S-like curve of approximately the same depth of switch and (ii) the two S-like curves are positioned one above the other, forming a kind of "vertical" structure. These distinguishing features are due to the cavity enhancement factor $\mathcal{R}_z^{(\mathcal{N})}$.

When d_B grows, the O-like curve becomes smaller and more distant from the double-S-like curve. At about $d_B = 900$Å, the IOBR picture transforms into a pure IOB picture presented by line 2 in Fig. 12. With further increase of d_B, the picture remains a pure IOB picture and the two S-like curves become more distant from each other. Figure 12 shows that the depth of switch decreases with growing d_B until 1500 Å (line 3). As lines 2 and 3 show, their double-S-like curves are still quite "vertical" and the depth of switch of the S-like constituents is almost the same for $d_B \leqslant 1500$ Å. What happens with further increase of d_B?

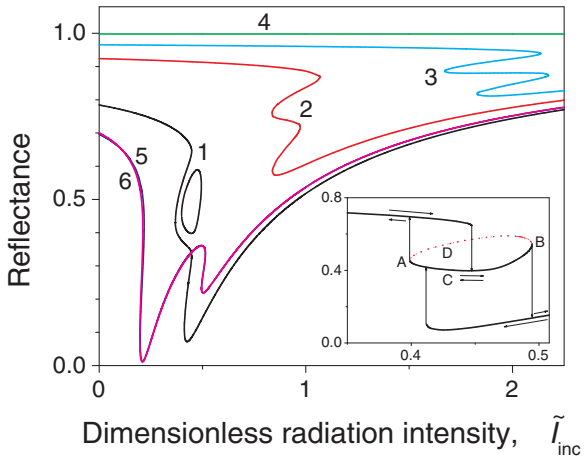

FIG. 12. (Color online) Dependence of reflectance on the dimensionless incident radiation intensity $\tilde{I}_{inc}$ for two-QW structure GaAs-AlAs(2.6 μm)-MQW-AlGaAs(3.85 μm)-air for different barrier thickness d_B with the corresponding MC eigenenergy $\hbar\omega_{MC}^{(n)}$: $d_B =$ 300 Å, $\hbar\omega_{MC}^{(1)} = 114.4$ meV (1), $d_B = 900$ Å, $\hbar\omega_{MC}^{(1)} = 109.6$ meV (2), $d_B = 1500$ Å, $\hbar\omega_{MC}^{(1)} = 105.1$ meV (3), $d_B = 8400$ Å, $\hbar\omega_{MC}^{(1)} =$ 72.2 meV (4), $d_B = 17\,430$ Å, $\hbar\omega_{MC}^{(2)} = 116.4$ meV (5), and $d_B =$ 34 700 Å, $\hbar\omega_{MC}^{(3)} = 116.7$ meV (6). Lines 5 and 6 practically coincide. Inset shows possible discontinuous transitions for the IOBR process that involves the O-like curve represented by line 1. Period for d_B is 51 770 Å. $\tilde{V}_{21} = 0.05$ and $N_S = 8\times10^{11}$ cm^{-2}.

Bearing in mind that the $Al_{0.33}Ga_{0.67}As$ barrier between two QWs functions as a spacer layer, a reader can ask if there is a value of d_B when the IOB picture practically transforms into a flat line with 100% reflectance and if there is a period for d_B that makes IOB pictures repeat themselves as in Fig. 10. Answers to both questions are positive. The IOB picture practically vanishes and becomes the flat line at $d_B = 8400$ Å (its depth of switch becomes 0.999–0.996 at the incident intensity of about 90). The d_B period is 51 770 Å which is practically the same as the period 51 750 Å for the frontier spacer layer. When d_B increases within the period interval from 300 to 52 070 Å, the pictures change three times from well-distinguished IOB to practically undetectable IOB, to pictures with no IOB at all and to well-distinguished IOB again, although the most vanishing flat-line picture occurs at $d_B = 8400$ Å.

The most pronounced IOB pictures with the deepest switch and the smallest $\tilde{I}_{inc}$ threshold (lines 1, 5, and 6) are associated with nearly resonant coupling of the incident radiation with the MC eigenmodes, in particular, lines 5 and 6 which practically coincide. A big difference between depths of switch for two S-like curves and a considerable distance between the S-like curves in lines 5 and 6 reveal that the QW which is closer to the AlAs mirror layer is located much closer to the antinode of the spatial intensity distribution than the other QW thanks to the big d_B. We suggest that the remarkable difference between the IOB processes in the two QWs accounts for the absence of the IOBR picture for lines 5 and 6 contrary to line 1.

Three intervals where IOB pictures are well distinguished on the 52 070-Å-long period interval are about 2000 Å long each. It attracts attention that the numbers 17 430, 34 700, and 52 070 Å, which are standing for the special values of d_B when the IOB pictures are the best pronounced, are practically equidistant which is associated with nearly resonant coupling of the radiation with the MC eigenmodes and particular symmetric location of the QWs in the eigenmodes' field.

Before investigating how a change of the thickness d_{SPAC} of the frontier GaAs spacer layer affects OB pictures, we have to set a constant value for d_B. Inspection of Fig. 12 shows that 900 Å is the smallest d_B with a pure IOB picture for $d_{SPAC} = 3.85$ μm. Considering the barrier as a spacer layer, one can suggest that there is supposed to be the smallest total thickness of spacer layers in the system to provide a pure IOB picture. Taking into account that $d_{SPAC} = 3.85$ μm provides the most pronounced IOB picture (see Fig. 10), one can suggest that assuming constant $d_B = 900$ Å would limit our opportunity to find conditions for the most pronounced IOB picture by a possibility of only increasing d_{SPAC}, which makes IOB pictures less pronounced. That is why we choose $d_B = 1500$ Å so that we can increase or decrease d_{SPAC} with regard to 3.85 μm. Figure 13 demonstrates that our suggestion is very fruitful. Well-distinguished IOB pictures are provided when d_{SPAC} falls in the interval around 3.465–3.85 μm.

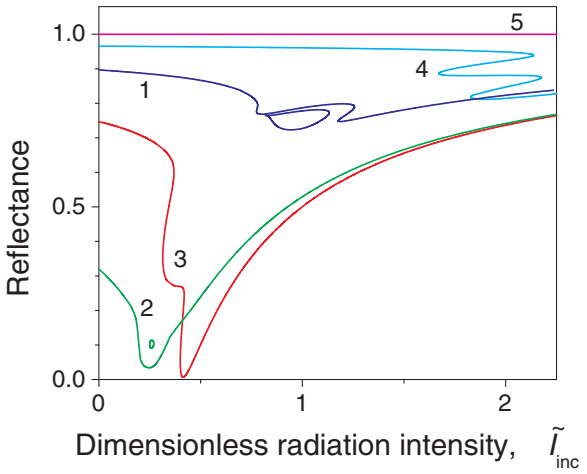

FIG. 13. (Color online) Dependence of reflectance on the dimensionless incident radiation intensity $\tilde{I}_{inc}$ for two-QW structure GaAs-AlAs(2.6 μm)-MQW-AlGaAs(d_{SPAC})-air with the same d_B = 1500 Å for different spacer-layer thickness d_{SPAC} with the corresponding MC eigenenergy $\hbar\omega_{MC}^{(n)}$: $d_{SPAC} = 2.6$ μm, $\hbar\omega_{MC}^{(1)} = 146.6$ meV (1), $d_{SPAC} = 3.3$ μm, $\hbar\omega_{MC}^{(1)} = 120$ meV (2), $d_{SPAC} = 3.465$ μm, $\hbar\omega_{MC}^{(1)} = 115.1$ meV (3), $d_{SPAC} = 3.85$ μm, $\hbar\omega_{MC}^{(1)} = 105.1$ meV (4), and $d_{SPAC} = 4.88$ μm, $\hbar\omega_{MC}^{(1)} = 85.7$ meV (5). Period for d_{SPAC} is 5.175 μm. $\tilde{V}_{21} = 0.05$ and $N_S = 8\times10^{11}$ cm^{-2}.

The most pronounced IOB picture associated with nearly resonant radiation coupling to the MC eigenmode occurs at $d_{SPAC} = 3.465$ μm. Pictures repeat themselves when d_{SPAC} changes with period of 5.175 μm. Our simulations show that there is only one value of d_{SPAC} on the period interval that provides the most pronounced IOB picture, contrary to the case with varying d_B in Fig. 12 that is expected due to rather small d_B compared with the distance between the mirrors. The IOBR picture with a highly asymmetric 8-like curve represented by line 1 stands for the case when both QWs are located close to each other in the proximity of the antinode of the spatial intensity distribution that provides similar but yet quite different IOB processes in each QW at nearly the highest possible intensity. Line 2 features the hidden IOB with no S-like curve for reflectance, with the O-like curve appearing due to similarity of the processes in two QWs at the nearly highest possible light intensity. For line 2, the radiation reflection in MC causes transformation of an S-like curve into a non-S-like curve as well as emergence of an O-like curve. A reader may have noticed that, compared to an 8-like curve, an O-like curve is associated with a process that occurs at a smaller $\tilde{I}_{inc}$ threshold and with a much deeper drop of reflectance due to MC.

3. *Many-QW-MC system*

Now, we see how IOB pictures work in systems of MQW-MC with three, five, and ten QWs. We choose such values for d_{SPAC} and d_B at constant d_{MIRR} that provide the most profound IOB pictures in each case. Line 1 in Fig. 14(a) represents the IOB process in the three-QW system, with the radiation field most enhanced by the MC, when the switch is the deepest and the threshold for $\tilde{I}_{inc}$ is the smallest. Note that each of the three QWs features an S-like curve similar to the one represented by line 9 in Fig. 10. Relatively small values of d_B account for the "vertical" structures of the IOB pictures in Figs. 14(a) (line 1) and 14(b).

An increase of d_B and/or the number of QWs modifies the spatial distribution of intensity further from the eigenmode pattern that results in a shallower switch and a bigger $\tilde{I}_{inc}$ threshold and a transformation of the "vertical" structure of S-like curves into a series of S-like curves [as for line 2 in Fig. 14(a)]. For up to five QWs, the depth of switch looks rather detectible. However, operation may become quite questionable when one wants to use individual switches. For example, a reader can see that transitions inside two lowest S-like curves in Fig. 14(b) cannot happen. On the other hand, it may offer

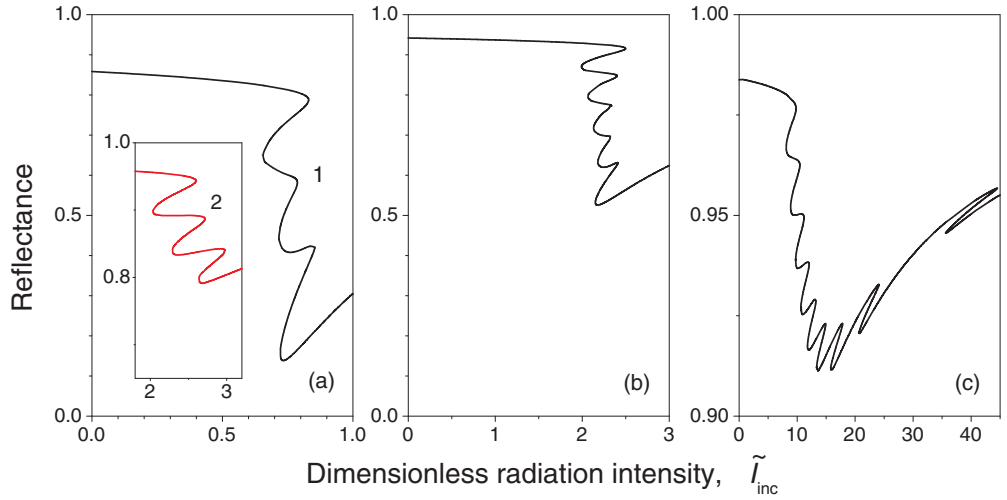

FIG. 14. (Color online) Dependence of reflectance on the dimensionless incident radiation intensity $\tilde{I}_{inc}$ for different numbers of QWs in GaAs-AlAs(2.6 μm)-MQW-AlGaAs(d_{SPAC})-air structure with the corresponding MC eigenenergy $\hbar\omega_{MC}^{(n)}$: (a) three QWs with $d_{SPAC} = 3.4$ μm, d_B = 1500 Å, and $\hbar\omega_{MC}^{(1)} = 112.3$ meV (1) and with $d_{SPAC} = 3.4$ μm, d_B = 2500 Å, and $\hbar\omega_{MC}^{(1)} = 102.4$ meV (2); (b) five QWs with d_{SPAC} = 3.1 μm, d_B = 1900 Å, and $\hbar\omega_{MC}^{(1)} = 105.5$ meV; and (c) ten QWs with $d_{SPAC} = 3.35$ μm, d_B = 1500 Å, and $\hbar\omega_{MC}^{(1)} = 88.9$ meV. Period for AlGaAs barrier is 5.177 μm. Period for AlGaAs spacer layer is 5.175 μm. $\tilde{V}_{21} = 0.05$ and $N_S = 8\times10^{11}$ cm^{-2}.

new opportunities. To make all S-like curves look like a series of switches, a wider barrier or a thicker spacer layer can be applied, but at the expense of decrease of the depth of switch. For smaller d_{SPAC} and d_{B} the pure IOB pictures in Fig. 14 modify into IOBR pictures.

Using the periodicity it is sometimes possible by manipulation of d_{SPAC} and d_{B} to get practically the same IOB pictures for different combinations of d_{SPAC} and d_{B}. For example, the IOB picture in Fig. 14(b) can be obtained as for $d_{\mathrm{SPAC}} = 3.1$ μm and $d_{\mathrm{B}} = 1900$ Å as for $d_{\mathrm{SPAC}} = 2.88$ μm and $d_{\mathrm{B}} = 2300$ Å.

Figure 14(c) demonstrates that for ten QWs, the IOB picture is not practically functional because of very small depth of switch. For bigger numbers of QWs, the depth of switch becomes smaller. Reflectance for MQW-MC with such big numbers of QWs becomes close to one which is different from the corresponding MQW-HMC case when reflectance is close to zero for some interval of intensity of the incident radiation (see Fig. 9). The difference comes from the fact that, contrary to the MQW-HMC structures, in the MQW-MC structures the peak intensity at the antinode of the spatial intensity distribution can change radically when thicknesses of the spacer layers vary. Alternation of the reflectance decrease (until $\tilde{I}_{\mathrm{inc}}$ is up to around 15) with the following reflectance increase in Fig. 14(c) has the same reason as for MQW-HMC systems. Thus, as in the case of MQW-HMC, MQW-MC with a few QWs rather than with many QWs seems to be more preferable from a practical point of view.

C. Interpretation of OB pictures

In this section, we want to take a deeper insight into the presented IOB pictures. In part, we discuss if the 8-like and O-like curves are experimentally observable and present possible discontinuous transitions by means of vertical straight lines with arrows in the insets of Figs. 5(b) and 12.

First of all, to help a reader interpret any of the displayed here IOB pictures with S-like, double-S-like, and multiple-S-like curves, we display in the inset b1 of Fig. 5(b) the discontinuous transitions (or switches) that can take place in the course of the forward (when $\tilde{I}_{\mathrm{inc}}$ increases) and backward (when $\tilde{I}_{\mathrm{inc}}$ decreases) processes for the double-S-like curve. A curious reader may have reasonable questions: Why are the discontinuous transitions assumed to occur exactly in the displayed way only? Why are no other switches between the upper and lower parts of the S-like curve assumed? The answer comes from the fact established in Ref. [19] that the assumed in the inset b1 discontinuous transitions during the IOB process are actually the resonant transitions when $\triangle\rho_{12}\tilde{V}_{21} \rightarrow \tilde{\delta}_{21}$ which is illustrated by our Eq. (18). Therefore, the discontinuous transitions between the switch points of the S-like curves displayed in the inset b1 are assumed to be overwhelmingly probable and outstanding among any other transitions.

As a reader may have already noticed from the presented figures, double-S curves are more various in shapes for MQW-MC systems than for MQW-HMC systems. Line 3 in Fig. 12 represents two successive switches for the forward IOB process and two successive switches for the backward IOB process. On the other hand, line 2 in Fig. 12, although it is a double-S-like curve, in reality represents only one switch. It is even more outstanding in Fig. 14(b) when five successive S-like curves factually represent only one switch for the forward IOB process. It profoundly manifests that the IOB in a MQW system is an integrated process of the entire system when contribution of an individual QW cannot be considered separately. On the whole, a reader can see that MQW-MC systems offer wide opportunities to design well-pronounced IOB pictures of different shapes.

Now, we would like to address a particular issue about the closed curves in the presented figures. We see 8-like curves in Figs. 5, 6, and 13. O-like curves are seen in Figs. 12 and 13. The question is: Can these closed curves be observed in experiment? Here, we can only speculate about it. First of all, what is the basic requirement for an 8-like curve or an O-like curve to appear in simulations? The considered system must have two (or more) QWs. 8-like and O-like curves do not appear in one-QW structures. Thus, an 8-like curve or an O-like curve accompanies a double-S-like curve (or a multi-S-like curve). As is mentioned, necessity of the second QW means necessity of the second special interface in the system of many interfaces: a sheet of Q2DEG. One sheet of Q2DEG forms an IOB picture, two sheets of Q2DEG form an IOBR picture.

We know that S-like curves are certainly observed. An S-like curve implies a switch between the switch points of the upper and lower parts of the "S." Can a closed curve that is completely separate from a double-S-like curve in an IOBR picture be observed experimentally? Taking into account that an 8-like curve is made by two S-like curves, we can suggest that an 8-like curve can be observed experimentally when an 8-like curve is (very) close to a double-S-like curve at the switch points of the double-S-like curve as it takes place in Figs. 5(c) and 5(b). Then, switch can occur from the switch points of a double-S-like curve to an 8-like curve and back. We can also suggest that the O-like curve in the IOBR picture presented by line 1 in Fig. 12 can be experimentally observed because there seems to be a possibility of switching from the switch points of the double-S-like curve to the O-like curve and back.

Now, we are going to draw discontinuous transitions for 8-like and O-like curves. Inset b2 in Fig. 5(b) reveals a complicated picture when an 8-like curve is involved. First, one needs to answer the following question: Which part of an 8-like curve is measurable (or stable) and which is nonmeasurable (unstable)? This question is open for suggestions. We suggest it is reasonable to assume that the part between points A and B is measurable. Also, we assume that the rest of the 8-like curve is not measurable. The reason for our assumption is that part AB in inset b1 is the closest to part AB in inset b2. It is energetically cheaper for the two-state electron system to execute the closest although different electron transitions. (In Ref. [19], the IOB process is treated within the framework of phase transition approach. Due to discontinuous transitions, there are formed assemblies, or phases, of electrons of the same state. Different types of discontinuous transitions allow formation of different phases. It is cheaper energetically for the system to form phases that are more similar rather than more different.) The situation becomes more ambiguous when it comes to a picture that involves an O-like curve. Out of two parts, ACB and ADB, that form the O-like curve in the inset in Fig. 12, we assume the ACB part to more likely participate in the discontinuous transitions. Our reason is the same as above

for the 8-like curve: the ACB part of the O-like curve is closer to the AB part of the double-S-like curve [see insert b1 in Fig. 5(b)].

In addition, there is dynamics of IOBR pictures with changing thickness of the structures that we see in our simulations. An O-like curve appears apart from one S-like part of a double-S-like curve. An O-like curve does not overlap with a double-S-like curve. An O-like curve can transform into an 8-like curve with changing thickness of a spacer layer as it is seen in Fig. 13 (lines 2 and 1). An 8-like curve can overlap with a double-S-like curve. An 8-like curve can be seen as two joined O-like curves. By manipulating the thickness of different layers, one can design an IOBR picture with a complicated and rather exotic combination of a double-S-like curve and a closed curve that can possibly be observed experimentally. Then the question is as follows: How to interpret such an IOBR picture? For example, line 1 in Fig. 12 or Figs. 5(b) or 5(c). If we represent each discontinuous change of the reflectance by a switch, then maybe the IOBR picture can be seen as a combination of four switches: a pair of switches connected in series is connected in parallel with another pair of switches connected in series? Here, we are left with a crucially important question: Which possibility will be realized every time the process is run? Is that system too exotic to operate practically?

As our numerical results demonstrate, the IOBR pictures occur for two-QW and multi-QW systems when each of the QWs features a very similar IOB picture, namely, very similar depth of switch and $\tilde{I}_{\rm inc}$ interval. Such conditions are met when the QWs are located usually close to each other near one antinode or at different antinodes of the spatial distribution of the radiation intensity. That is why the IOBR pictures occur usually at small $\tilde{I}_{\rm inc}$ and small $d_{\rm B}$. It is fruitful to see the pictures in the realm of time when $\tilde{I}_{\rm inc}$ grows with time. For example, Fig. 5(a) shows that one IOB process occurs first in the first QW and later a similar IOB process occurs in the second QW under the condition when the reflectance of the system is already changed by the previous IOB process that reveals interdependence of the two well spatially and temporally resolved IOB processes. On the other hand, two very similar IOB processes occur practically simultaneously in both QWs for Fig. 5(c) when a discontinuous change of $\triangle\rho_{12}$ takes place in both QWs simultaneously. A jump of $\triangle\rho_{12}$ in one QW changes reflectance of the system that in turn changes conditions [namely, the value of $\tilde{I}_z$ and therefore the factor b in the cubic equation (9)] for a jump of $\triangle\rho_{12}$ in the other QW and vice versa. Technically, each QW has a set of three different real solutions of the cubic equation simultaneously, with the solutions for one QW changing the cubic equation for the other QW and vice versa so that the solutions for two QWs become different. As a result, at the same $\tilde{I}_{\rm inc}$ simultaneously there are two different sets of three different real values for $\triangle\rho_{12}$ that are represented by the double-S-like curve and 8-like curve in Fig. 5(c). Such interaction of two similar but a bit different IOB processes in two identical QWs resembles the wave beats effect. We call it the IOB beats effect. By this analogy we suggest that in the case of Fig. 5(c), both the double-S-like curve and the 8-like curve can be observed experimentally when some electrons are governed by one of the curves and some electrons by the other curve. We suggest that energetically it is cheaper that the double-S-like curve and the 8-like curve are realized spatially separately in different QWs. Note that when the number of QWs grows, a possibility of having the IOB beats effect in some neighbor QWs increases. We observe IOBR pictures for MQW systems with big numbers of QWs.

Finally, a reader may have already noticed a major challenge for experimental observation of the IOBR pictures and IOB beats effect. We assume that two IOB processes in QWs are supposed to be rather close to each other to produce the IOB beats. The challenge is to detect the difference between them like the one between the line AB in inset b1 and line AB in inset b2 in Fig. 5(b). One can see that the IOB beats effect displayed in Fig. 5(c) is not detectable experimentally. A reasonable, although little, difference between IOB processes is required for the experimental observation.

D. QWs in an infinite material environment

To get a deeper insight into how the IOB pictures are produced by the Q2DEG and modified by multiple light reflection from interfaces, we present IOB pictures for systems of one and two identical QWs sandwiched between two semi-infinite GaAs claddings (the transmission geometry) for $\varphi = 65^\circ$.

Line 1 in Fig. 15 that is well described by Eq. (19) shows that when one QW is located in a homogeneous GaAs space (with the same dielectric constant 10.89 throughout the entire space), the QW features a pure IOB phenomenon represented by one S-like curve merely due to the nonlinear properties of the 2D electrons. Lines 2 to 5 in Fig. 15 demonstrate that incorporation of difference between dielectric constants of the QW and the barrier makes the S-like curves more distinct, in particular, it increases the depth of switch and reduces the $\tilde{I}_{\rm inc}$ threshold. This is a result of formation of a standing-

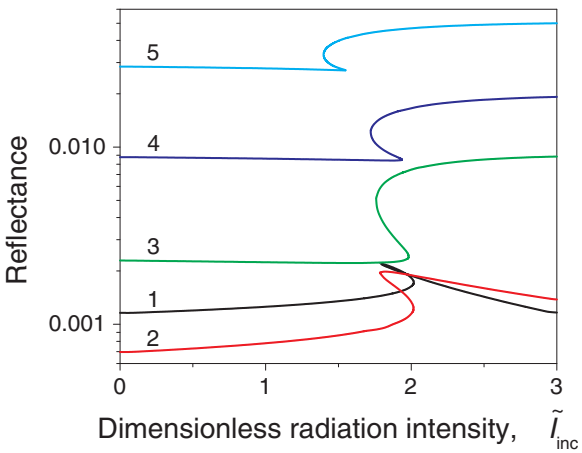

FIG. 15. (Color online) Dependence of reflectance on the dimensionless incident radiation intensity $\tilde{I}_{\rm inc}$ for one-QW system sandwiched between two half-spaces of GaAs in GaAs-QW-GaAs structure for different barrier thickness $d_{\rm B}$: $d_{\rm B} = 300$ Å (2) and $d_{\rm B} = 3000$ Å (3), $d_{\rm B} = 5000$ Å (4) and $d_{\rm B} = 15\,000$ Å (5). Line 1 represents the case when the same dielectric constant 10.89 is assumed throughout the entire structure. For the case of $\varepsilon_w = 10.89$ and $\varepsilon_b = 9.989$, the period for $d_{\rm B}$ is 51 770 Å. $\tilde{V}_{21} = 0.05$ and $N_{\rm S} = 8\times10^{11}$ cm^{-2}.

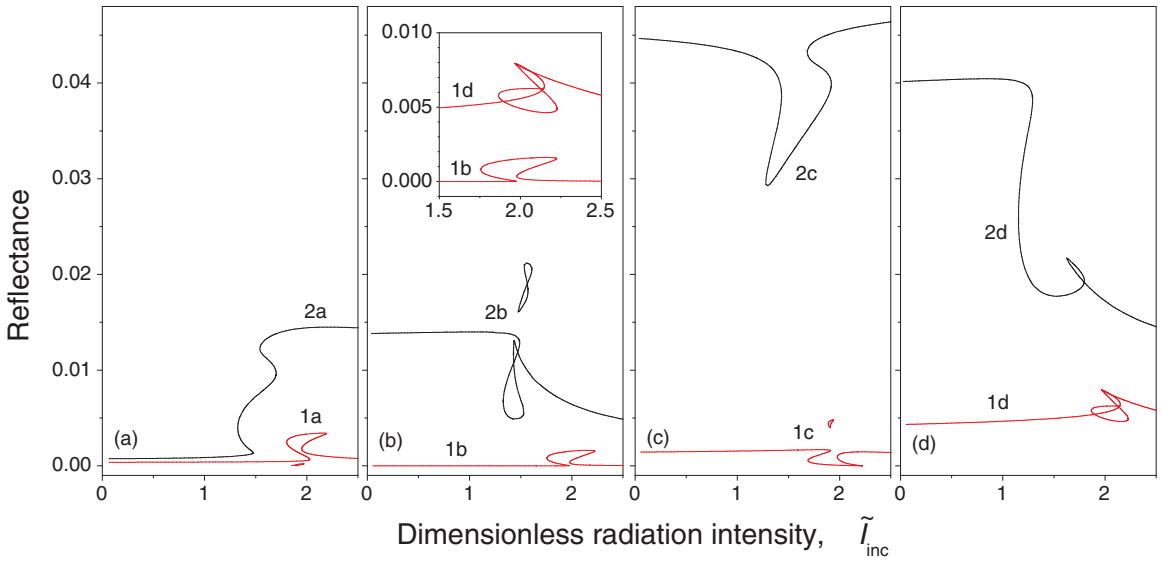

FIG. 16. (Color online) Dependence of reflectance on the dimensionless incident radiation intensity $\tilde{I}_{inc}$ for two-QW system sandwiched between two half-spaces of GaAs in GaAs-MQW-GaAs structure for different barrier thickness d_B: $d_B = 15\,000$ Å (a), $d_B = 18\,960$ Å (b), $d_B = 25\,885$ Å (c), and $d_B = 37\,920$ Å (d). Line 1d also describes the case of $d_B = 0$. Lines 1a, 1b, 1c, and 1d represent the case when the same dielectric constant 10.89 is assumed throughout the entire structure. Lines 2a, 2b, 2c, and 2d stand for $\varepsilon_w = 10.89$ and $\varepsilon_b = 9.989$. For the case of $\varepsilon_w = 10.89$ and $\varepsilon_b = 9.989$, the period for d_B is 51 770 Å. For $\varepsilon_w = \varepsilon_b = 10.89$, the period for d_B is 37 920 Å. $\tilde{V}_{21} = 0.05$ and $N_S = 8\times10^{11}$ cm^{-2}. In the inset: lines 1b and 1d zoomed in.

wave pattern by light reflection from the newly created GaAs-GaAlAs interfaces. Our simulations show that IOB pictures for the one-QW structure with $\varepsilon_w = 10.89$ (GaAs) and $\varepsilon_b = 9.989$ (AlGaAs) repeat themselves when d_B changes with the period of 51 770 Å, which proves the existence of the pattern.

IOB pictures become even more intriguing when we take two-QW systems in the infinite material space. Our analytical calculations and computer simulations show that due to the light reflection from Q2DEG, a standing-wave pattern is formed even by only two parallel sheets of Q2DEG placed into an infinite medium with constant dielectric constant. Period for d_B is observed to have IOB pictures repeat themselves. For the homogeneous GaAs medium, the period is 37 920 Å. IOB pictures change dramatically with varying d_B as is illustrated by lines 1a, 1b, 1c, and 1d in Fig. 16 where line 1d represents the picture at the beginning ($d_B = 0$) and at the end ($d_B = 37\,920$ Å) of the period interval and line 1b exactly at the center ($d_B = 18\,960$ Å) of the interval. Line 1b features a double-S-like curve of the pure IOB process and lines 1a, 1c, and 1d do IOBR pictures. For the vanishing separation d_B, the IOB processes in each of two Q2DEG sheets are practically the same, which produces a pronounced IOBR picture for line 1d that consists of an S-like curve and an 8-like curve, with the S-like curve is exactly the IOB picture for one sheet of Q2DEG with the doubled oscillator strength (line 1 in Fig. 15 multiplied by 4) and one loop of the 8-like curve coincides with a part of the S-like curve. The amplitude of the standing-wave pattern is so small that the radiation intensities at two Q2DEG sheets do not differ much at any given $\tilde{I}_{inc}$. The IOBR condition (21) is not met only around $d_B = 18\,960$ Å (line 1b) when Q2DEG sheets are separated by a half wavelength of the pattern that makes the intensity difference the biggest.

When the QW material and the barrier material are assumed to have different dielectric constants of GaAs and AlGaAs, respectively, the standing-wave pattern modifies essentially that results in radical change of the IOB pictures as is demonstrated by lines 2a, 2b, 2c, and 2d in Fig. 16. Period for d_B is 51 770 Å. Reflectance increases due to additional GaAs-GaAlAs interfaces. S-like curves demonstrate deeper switch and smaller $\tilde{I}_{inc}$ threshold due to bigger amplitude of the standing-wave pattern. It is interesting that line 1d represents the IOBR picture at the edges of the period interval as for $\varepsilon_w = \varepsilon_b$ ($d_B = 37\,920$ Å) as for $\varepsilon_w \neq \varepsilon_b$ ($d_B = 51\,770$ Å). The system manifests a pronounced IOB picture by line 2c in the middle of the first period interval due to the biggest difference between the radiation intensities at the Q2DEG sheets.

It attracts attention that the S-like and double-S-like curves in Figs. 2–16 have various shapes. For one-QW systems in HMC and MC, we have observed the same type of a reverse S-like curve that is the only possible type for layered structures with the total reflection. Each QW in MQW-HMC and MQW-MC also features only a reverse S-like curve that lets us introduce a concept of "effective" QW for MQW systems. The situation is different for the transmission geometry. Figure 15 demonstrates the only possible type of an S-like curve for the IOB process in one QW that differs from the total reflection geometry case. Figure 16 shows that each of two QWs can feature a different S-like curve. In part, double-S-like curves can be in a form of a "wall" (line 1b) or a "well" (line 1c). The key reason for the difference is how the standing-wave pattern of the radiation intensity distribution is determined. For the MQW-HMC and MQW-MC, it is the mirrors that mainly define the patterns. For the transmission geometry with $\varepsilon_w = \varepsilon_b$, the pattern is fully defined by two sheets of Q2DEG which are radically changing their properties under the IOB regime. Note that for, say, $\tilde{I}_{inc} = 2.5$, both QWs have $\triangle\rho_{12}(\tilde{I}_z) < 0.4$ [see the inset in Fig. 2(c)] for all lines in Fig. 16.

A reader may be curious as to why one Q2DEG sheet features an S-like curve and the other Q2DEG sheet features a reverse S-like curve to counter each other in lines 1a, 1b, and 1c in Fig. 16. Why do not the both sheets feature a series of two S-like curves like the one in line 2a or a series of two reverse S-like curves like that in Fig. 5(a)? One can notice for lines 1a, 1b, and 1c that reflectance beyond the "wall" or "well" IOB area is flat and the "wall" or "well" shifts the value of that flat reflectance. The reflectance is flat when both Q2DEG sheets have practically the same properties. It is true for smaller $\tilde{I}_{\rm inc}$ before the "wall" or "well" when $\triangle\rho_{12}(\tilde{I}_z) > 0.7$ for both Q2DEG sheets. It is also true for bigger $\tilde{I}_{\rm inc}$ after the "wall" or "well" when $\triangle\rho_{12}(\tilde{I}_z) < 0.4$ for both sheets. In the "wall" or "well" area, one sheet has $\triangle\rho_{12}(\tilde{I}_z) < 0.4$ and the other sheet has $\triangle\rho_{12}(\tilde{I}_z) > 0.7$, which makes the sheets quite different and results in a considerable change of reflectance compared to the flat reflectance beyond the IOB area. An important element in such a mechanism is a rather small absorption of the Q2DEG sheets so that the flat reflectance does not change much by discontinuous change of absorptive properties of both Q2DEG sheets. The value of the flat reflectance is determined by the location of the sheets in the standing-wave pattern. It is the lowest, practically zero, when the sheets are separated by $d_{\rm B}$ equal to the half wavelength of the pattern that makes the two Q2DEG sheets produce a "wall" form of the IOB area in line 1b because a "well" form is not possible. When the flat reflectance is big enough, two Q2DEG sheets make a "well" form in line 1c.

Incorporation of GaAs-GaAlAs interfaces dramatically changes the standing-wave pattern, in part its amplitude. But, the most important is that the Q2DEG sheets are no longer the full controllers of the pattern. It brings a wide variety of IOB pictures. The IOB pictures in Fig. 16 unambiguously demonstrate that the IOB processes in the QWs are completely interdependent.

Finally, although Figs. 15 and 16 do not seem to be practical for applications, they, however, seem to be very illustrative to represent in the clearest way the title of this work.

IV. CONCLUSIONS

In this work, we have theoretically investigated the nonlinear (saturated) intersubband response, in particular the intrinsic optical bistability, of quantum well structures, in part those embedded in microcavities. A semiclassical approach is employed that is based on the plane-wave approximation, the transfer-matrix formalism, the sheet model, and the density-matrix formalism developed to calculate the 2D nonlinear intersubband electron conductivity and the IOB.

A variety of presented numerical results demonstrate basic features of the IOB in QW structures. Particular attention is paid to the effect of radiation reflection from different interfaces in MQW systems on the IOB process. It is shown that knowing a spatial distribution of radiation intensity in the layered structures, in part standing-wave patterns and eigenmodes of MC, is crucial for understanding of IOB pictures. The IOB in systems of one, two, three, five, and ten QWs is investigated. The multistability phenomenon is addressed. The presented finding can be useful for the design of QW structures to operate IOB regimes.

[1] F. A. Hopf, C. M. Bowden, and W. H. Louisell, Phys. Rev. A **29**, 2591 (1984).

[2] P. M. Mejias, R. Martinez-Herrero, and E. Bernabeu, Appl. Opt. **24**, 2092 (1985).

[3] M. Zaluzny, Phys. Rev. B **47**, 3995 (1993); J. Appl. Phys. **74**, 4716 (1993).

[4] K. Craig, B. Galdrikian, J. N. Heyman, A. G. Markelz, J. B. Williams, M. S. Sherwin, K. Campman, P. F. Hopkins, and A. C. Gossard, Phys. Rev. Lett. **76**, 2382 (1996).

[5] A. A. Batista, P. I. Tamborenea, B. Birnir, M. S. Sherwin, and D. S. Citrin, Phys. Rev. B **66**, 195325 (2002).

[6] H. O. Wijewardane and C. A. Ullrich, Appl. Phys. Lett. **84**, 3984 (2004); Phys. Status Solidi C **3**, 2498 (2006).

[7] S. G. Kosionis, A. F. Terzis, C. Simserides, and E. Paspalakis, J. Appl. Phys. **108**, 034316 (2010).

[8] S. G. Kosionis, A. F. Terzis, C. Simserides, and E. Paspalakis, J. Appl. Phys. **109**, 063109 (2011).

[9] I. Karabulut, J. Appl. Phys. **109**, 053101 (2011).

[10] A. Liu and O. Keller, Opt. Commun. **120**, 171 (1995).

[11] M. Zaluzny and W. Zietkowski, Phys. Rev. B **88**, 195408 (2013).

[12] T. Shih, K. Reimann, M. Woerner, T. Elsaesser, I. Waldmuller, A. Knorr, R. Hey, and K. H. Ploog, Phys. Rev. B **72**, 195338 (2005); Phys. E (Amsterdam) **32**, 262 (2006).

[13] X. Chen, J. Opt. B: Quantum Semiclass. Opt. **1**, 524 (1999).

[14] A. A. Batista and D. S. Citrin, Opt. Lett. **29**, 367 (2004).

[15] K. L. Vodopyanov, V. Chazapis, C. C. Phillips, B. Sung, and J. S. Harris Jr, Semicond. Sci. Technol. **12**, 708 (1997).

[16] R. Steed, M. Matthews, J. Plumridge, M. Frogly, C. Phillips, Z. Ikonic, P. Harrison, O. Malis, L. N. Pfeffer, and K. W. West, Appl. Phys. Lett. **92**, 183104 (2008).

[17] M. Załużny and C. Nalewajko, Phys. Rev. B **59**, 13043 (1999).

[18] M. Załużny and C. Nalewajko, J. Appl. Phys. **107**, 123106 (2010).

[19] Victor Bondarenko, http://elibrary.wayne.edu/record=b3626506~S47

[20] M. Załużny and C. Nalewajko, Phys. Rev. B **68**, 233305 (2003).

[21] E. J. Roan and S. L. Chuang, J. Appl. Phys. **69**, 3249 (1991).

[22] K. L. Campman, H. Schmidt, A. Imamoglu, and A. C. Gossard, Appl. Phys. Lett. **69**, 2554 (1996).

[23] R. A. Kaindl, K. Reimann, M. Woerner, T. Elsaesser, R. Hey, and K. H. Ploog, Phys. Rev. B **63**, 161308 (2001).

[24] M. Załużny and C. Nalewajko, J. Appl. Phys. **99**, 026104 (2006).